Efficient cytosolic delivery of luminescent lanthanide bioprobes in live cells for two-photon microscopy

Kyangwi Malikidogo, Thibault Charnay, Daouda Ndiaye, Ji-Hyung Choi, Lucile Bridou, Baptiste Chartier, Sule Erbek, Guillaume Micouin, Akos Banyasz, Olivier Maury, et al.

Chemical Science

ROYAL SOCIETY OF CHEMISTRY

EDGE ARTICLE

View Article Online
View Journal | View Issue

Cite this: *Chem. Sci.*, 2024, **15**, 9694

All publication charges for this article have been paid for by the Royal Society of Chemistry

Efficient cytosolic delivery of luminescent lanthanide bioprobes in live cells for two-photon microscopy†

Kyangwi P. Malikidogo, ‡§[ab] Thibault Charnay,‡[ab] Daouda Ndiaye,[a] Ji-Hyung Choi,[a] Lucile Bridou,[c] Baptiste Chartier,[a] Sule Erbek,[de] Guillaume Micouin,[c] Akos Banyasz, [c] Olivier Maury, [c] Véronique Martel-Frachet, [de] Alexei Grichine [d] and Olivier Sénèque *[a]

Received 6th February 2024
Accepted 26th April 2024

DOI: 10.1039/d4sc00896k

rsc.li/chemical-science

Lanthanide(III) (Ln^{3+}) complexes have desirable photophysical properties for optical bioimaging. However, despite their advantages over organic dyes, their use for microscopy imaging is limited by the high-energy UV excitation they require and their poor ability to cross the cell membrane and reach the cytosol. Here we describe a novel family of lanthanide-based luminescent probes, termed dTAT[Ln·L], based on (i) a DOTA-like chelator with a picolinate moiety, (ii) a two-photon absorbing antenna to shift the excitation to the near infrared and (ii) a dimeric TAT cell-penetrating peptide for cytosolic delivery. Several Tb^{3+} and Eu^{3+} probes were prepared and characterized. Two-photon microscopy of live cells was attempted using a commercial microscope with the three probes showing the highest quantum yields (>0.15). A diffuse Ln^{3+} emission was detected in most cells, which is characteristic of cytosolic delivery of the Ln^{3+} complex. The cytotoxicity of these three probes was evaluated and the IC_{50} ranged from 7 μM to >50 μM. The addition of a single positive or negative charge to the antenna of the most cytotoxic compound was sufficient to lower significantly or suppress its toxicity under the conditions used for two-photon microscopy. Therefore, the design reported here provides excellent lanthanide-based probes for two-photon microscopy of living cells.

Introduction

Fluorescence microscopy is an essential tool in biological research[1] and among the various techniques, Laser Scanning Confocal Microscopy (LSCM), which allows imaging of a cell section and 3D reconstruction of cells, is one of the most popular techniques today.[2,3] LSCM has prompted the development of genetically encoded fluorescent proteins or synthetic cell-permeable molecular fluorescent dyes to reveal subcellular components or monitor biological processes.[4–6] The first fluorophores used for LSCM required high-energy excitation in the UV-blue optical window, which damages cells. This led to the development of two-photon microscopy (2PM),[7] a technique based on two-photon (2P) excited fluorescence, in which excitation of the molecule is caused by simultaneous absorption of two photons of equal energy, half the energy required for single photon (1P) excitation. Consequently, instead of being excited in the UV-blue window, 2P-absorbing dyes are excited with near-infrared (NIR) light, which is less energetic and therefore less damaging to cells. In addition, NIR light penetrates deeper into the biological tissues.[8] Since 2P excitation happens only in a very small volume corresponding to the focal point of the pulsed laser source, 2PM is comparable to LSCM in its ability to image cell sections, but superior to LSCM for imaging live cells or thick biological samples due to the NIR excitation. Over the past two decades, numerous organic fluorescent dyes have been developed that are suitable for 1P or 2P excitation in the red-NIR window, but in many cases they suffer from a lack of photostability, poor water solubility and low cell penetration capacity.[9–11]

Complexes of trivalent lanthanides (Ln^{3+}) exhibit interesting luminescence properties for biological applications, making

[a]*Univ. Grenoble Alpes, CNRS, CEA, IRIG, LCBM (UMR 5249), F-38000 Grenoble, France. E-mail: olivier.seneque@cea.fr*

[b]*Univ. Grenoble Alpes, CNRS, DCM (UMR 5250), F-38000 Grenoble, France*

[c]*Univ. Lyon, ENS de Lyon, CNRS UMR 5182, Laboratoire de Chimie, Lyon F-69342, France*

[d]*Univ. Grenoble Alpes, INSERM U1209, CNRS UMR 5309, Institute for Advanced Biosciences, F-38000 Grenoble, France*

[e]*EPHE, PSL Research University, 4-14 rue Ferrus, 75014 Paris, France*

† Electronic supplementary information (ESI) available: Procedures for the synthesis of protected macrocyclic ligands, peptide and conjugates and Ln^{3+} complexes; characterizations by 1P and 2P spectroscopy; protocols for cell culture, 2P microscopy and MTT proliferation assays. See DOI: https://doi.org/10.1039/d4sc00896k

‡ These authors contributed equally to this work.

§ Present address: Faculté des Sciences et Technologies, Université de Goma, B.P. 204 Goma, R. D. Congo.

them an attractive alternative to organic fluorescent dyes.[12–17] Each Ln^{3+} exhibits a fingerprint-like emission consisting of sharp atom-like emission bands at fixed wavelengths, independent of the environment, making them easily recognizable. Depending on the Ln^{3+}, these bands cover the visible and NIR. Ln^{3+} luminescence is characterized by long lifetimes (in the microsecond to millisecond range), allowing background fluorescence (in the nanosecond range) to be suppressed by time-gated detection. In addition, luminescent Ln^{3+} complexes are highly photostable compared to organic dyes. They have been widely used in biological assays based on homogenous time-resolved technology.

Despite these advantages, Ln^{3+} complexes are not routinely used by biologists for cell microscopy as compared to organic dyes. There are two reasons for this. First, due to the low extinction coefficient of the f–f transitions, Ln^{3+} luminescence must rely on the antenna effect to be effective: a light-harvesting chromophore located close to the Ln^{3+} cation is excited and transfers energy to the Ln^{3+} to bring it into its emitting excited state. However, the antenna chromophore usually requires UV excitation which is damaging to cells. To overcome this problem, it is possible to use Ln^{3+} complexes with 2P-absorbing push–pull antennas.[18–20] Importantly, it was demonstrated that 2PM with such Ln^{3+} complexes is possible with commercial microscopes commonly used by biologists.[21] However, most of these 2P-absorbing Ln^{3+} complexes fail to penetrate live cells and cell fixation was required prior to incubation with the Ln^{3+} probe in order to permeabilize the cell membrane and let the probe go into the cell.

The second reason against using Ln^{3+} complexes as dyes for LCSM or 2PM is their cell penetration and their cellular localization properties. Parker and co-workers have studied the cell uptake and localization of various Ln^{3+} complexes with cyclen-based macrocyclic chelator with appended antenna. Many of them are able to penetrate cells, either neutral, negatively or positively charged. Indeed, cell penetration seems not to depend on charge but rather on antenna nature and linkage.[22–26] Nevertheless, this cell uptake property does not apply to all Ln^{3+} complexes since other negatively charged cyclen-based Ln^{3+} complexes that we have recently described are unable to penetrate cell.[27] Parker and co-workers have performed LSCM of cells using numerous Ln^{3+} complexes with 1P excitation in the UV.[26,28,29] Most often, however, Ln^{3+} complexes end up in lysosomes or stick to the mitochondrial membrane.[26] They are not properly delivered to the cytosol. Furthermore, it is difficult to predict the subcellular localization of a Ln^{3+} complex on the basis of its molecular structure, as localization can be influenced by minor changes in the antenna or chelator moieties. A convenient solution to these problems would be to conjugate the Ln^{3+} complex to a cell-penetrating peptide (CPP). CPPs are short peptides, usually cationic, that enter cells either by direct membrane translocation or by endocytosis.[30] However, the CPP has to be chosen carefully, as many CPPs, whether natural such as TAT (transactivator of transcription of human immunodeficiency virus) or synthetic such as R8 (octa-arginine), do not effectively reach the cytosol.[31]

Ten years ago, Pellois and co-workers described a dimer of the TAT CPP, called dfTAT, with a (tetramethyl)rhodamine dye grafted onto each TAT monomer and dimerized by a disulfide bond (Fig. 1A).[32,33] dfTAT is internalized into living cells by endocytosis and promotes endosomal leakage so that the rhodamine fluorophore reaches the cytosol and spreads throughout the entire cell. Inspired by this work, we describe here a family of luminescent bioprobes, called dTAT[Ln·L], consisting of Ln^{3+} complex with 2P absorbing push–pull antennas conjugated to a TAT dimer (Fig. 1B). We demonstrate that they enable 2PM imaging of living cells thanks to the appropriate photophysical properties of the Ln^{3+} complexes and the efficient cytosolic delivery with the TAT dimer. In addition, we show that toxicity issues can be easily controlled by modulation of the antenna.

Results and discussion

Design of the probes

Two factors are important for efficient cytosolic delivery of the dfTAT system (Fig. 1A): (i) the high number and high density of arginines in the dimer and (ii) the hydrophobic aromatic core of the rhodamine dye. Therefore, we decided to evaluate whether replacing the rhodamine dye with a Ln^{3+} complex could provide a probe that reaches the cytosol, with the aromatic sensitizing

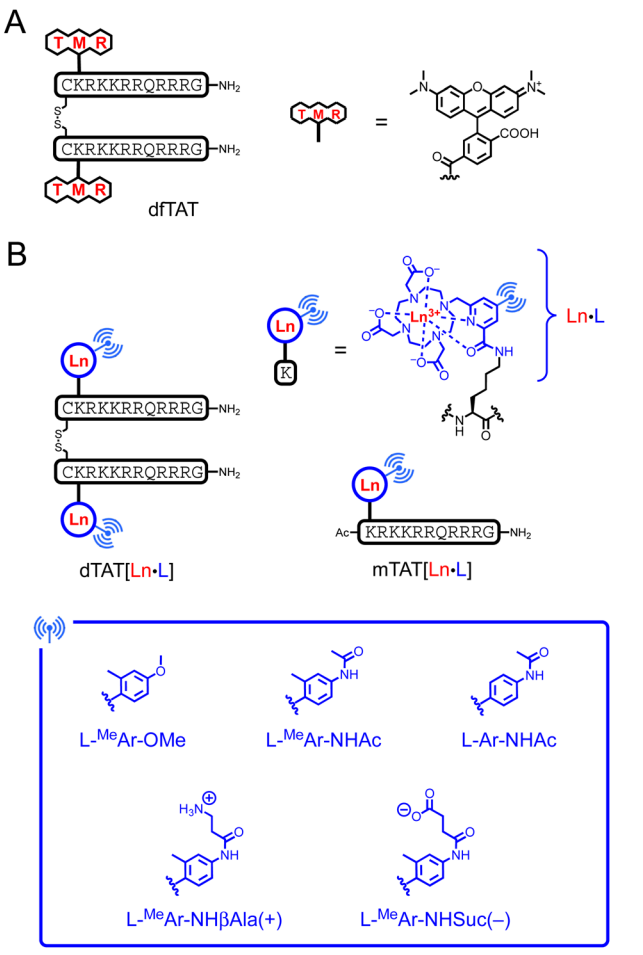

Fig. 1 Chemical structure of (A) dfTAT and (B) Ln^{3+}-based probes dTAT[Eu·L] and mTAT[Eu·L]. L denotes the DO3Apic macrocycle.

antenna playing the role of the rhodamine aromatic core in endosomal escape. As a Ln^{3+} ligand, we chose DO3Apic, a DOTA-type ligand in which one of the acetate arms has been replaced by a picolinate one. It forms stable complexes with Ln^{3+} that exhibit interesting luminescence properties, including long luminescence lifetimes and moderate to high quantum yields for Eu^{3+} and Tb^{3+}.[34] The addition of a π-conjugated system with an electron donating group to the picolinate antenna allows a red-shift of the excitation wavelength and an increase in the extinction coefficient for superior luminescence properties[27,35] and converts the picolinate into a push–pull antenna suitable for 2P absorption.[35] From a synthetic point of view, it is easy to distinguish the carboxylate of the picolinate from those of the acetates by playing with *tert*-butyl/methyl ester protection (see ESI†) in order to use it as a unique conjugation site for coupling to a peptide lysine side chain. Therefore, we decided to use the DO3Apic macrocycle as a Ln^{3+} ligand in the TAT dimer system. From our experience, we know that aryl-alkynyl-picolinate antennas, which are excellent for sensitizing Eu^{3+} luminescence, are not very stable under the conditions required for peptide synthesis (especially under the acidic conditions used for resin cleavage and deprotection steps) due to the addition of nucleophiles on the triple bond.[27] Therefore, we opted for aryl-picolinate antennas and three of them were evaluated (Fig. 1B). The first one has an *ortho*-methyl group and a *para*-methoxy, which acts as an electrodonating group in the push–pull system. It was previously shown that such an antenna sensitizes Tb^{3+} better than Eu^{3+}.[36] In the second antenna, the methoxy group is replaced by an acetamide moiety and in the third antenna, the *ortho*-methyl group is deleted compared to the second one. In order to characterize the luminescence properties of the corresponding Tb^{3+} and Eu^{3+} complexes, the six conjugates mTAT[Ln·L-^{Me}Ar-OMe], mTAT[Ln·L-^{Me}Ar-NHAc] and mTAT[Ln·L-Ar-NHAc] with Ln = Tb and Eu (Fig. 1B) were prepared. The Gd^{3+} analogues were also prepared to determine the energy of their excited triplet state. Their synthesis is described in the ESI.†

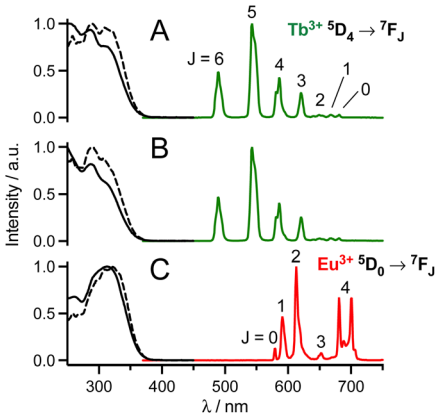

Fig. 2 Normalized 1P absorption (black solid line), 1P excitation (black dashed line; λ_{em} = 545 nm (A and B) or 615 nm (C)) and emission (coloured solid line; λ_{ex} = 315 nm) spectra of (A) mTAT[Tb·L-^{Me}Ar-OMe], (B) mTAT[Tb·L-^{Me}Ar-NHAc] and (C) mTAT[Eu·L-Ar-NHAc] in PBS.

Photophysical properties

The luminescence properties of the probes were evaluated in PBS (pH 7.4). Absorption, excitation and emission spectra are shown in Fig. 2 or in the ESI† and spectroscopic data are summarized in Table 1. Absorption spectra of mTAT[Ln·L] compounds show two bands at *ca.* 285 and 315 nm, which are attributed to locally excited (LE) and intra-ligand charge transfer (ILCT) transitions within the antenna, respectively.[27,36] In the case of twisted antennas, *i.e.* with an *ortho*-methyl group, the LE band dominates and the ILCT band appears as a shoulder while

Table 1 Spectroscopic characterizations in aerated PBS and cytotoxicity (IC_{50}) determined by MTT proliferation assay on HeLa cells[a]

Compound	λ_{max}; $\lambda_{cut\text{-}off}$/nm	$E(S_1)$; $E(T_1)$[b]/cm^{-1}	ε at λ_{max}/M^{-1} cm^{-1}	σ_{2P} at 700 nm/GM	Φ_{Ln}	τ_{Ln}/ms	IC_{50}/μM
mTAT[Ln·L-^{Me}Ar-OMe]	285; 363	S_1: 27 600 T_1: 22 900	16 000	5.7	Tb: 0.55 Eu: 0.040	Tb: 2.11 Eu: 1.05	
mTAT[Ln·L-^{Me}Ar-NHAc]	287; 361	S_1: 27 800 T_1: 22 700	14 000	4.2	Tb: 0.20 Eu: 0.048	Tb: 0.83 Eu: 1.05	
mTAT[Ln·L-Ar-NHAc]	315; 366	S_1: 27 300 T_1: 22 000	20 000	11.1	Tb: 0.027 Eu: 0.15	Tb: 0.07 Eu: 1.05	
dTAT[Tb·L-^{Me}Ar-OMe]	285, 366		32 000[a]		Tb: 0.38	Tb: 1.40	18 ± 3
dTAT[Tb·L-^{Me}Ar-NHAc]	288, 364		28 000[c]		Tb: 0.12	Tb: 0.46 (98%), 1.63 (2%)	7.6 ± 1.6
dTAT[Eu·L-Ar-NHAc]	317; 370		40 000[c]		Eu: 0.15	Eu: 1.08	>50
dTAT[Tb·L-^{Me}Ar-NHβAla(+)]	289, 366		30 000		Tb: 0.14	Tb: 0.34 (99%), 1,43 (1%)	22 ± 5
dTAT[Tb·L-^{Me}Ar-NHSuc(−)]	286, 368		26 000		Tb: 0.17	Tb: 0.46 (97%), 2.07 (3%)	>50

[a] Error on ε value is estimated ±5% on ε values and ±10% on Φ_{Ln} and σ_{2P}. Error on τ_{Ln} is estimated ±0.03 ms. [b] Energy of the excited triplet state is estimated from the wavelength at half-maximum on the onset of the time-gated phosphorescence spectrum of the Gd^{3+} analogue in PBS/glycerol 9 : 1 v/v recorded at 77 K. [c] Extinction coefficient ε of dimers are estimated twice that of the monomer with the same antenna.

in the case of the freely rotating antenna, *i.e.* in the absence of *ortho*-methyl, the ILCT band dominates the absorption. The ILCT band extends up to *ca.* 365 nm ($\lambda_{cut\text{-}off}$ in Table 1).

Excitation into these bands yields characteristic Tb^{3+} $^5D_4 \rightarrow {}^7F_J$ (J = 6–0) or Eu^{3+} $^5D_0 \rightarrow {}^7F_J$ (J = 0–4) emissions in the 450–750 nm range. The excitation spectra match the absorption spectra, which confirms sensitization of Ln^{3+} luminescence by antenna effect. Interestingly, with respect to quantum yields of Ln^{3+} emission, the antenna with the *ortho*-methyl group sensitizes Tb^{3+} better while the one without the *ortho*-methyl group sensitizes Eu^{3+} better.[36] Quantum yields and lifetimes of Tb^{3+} emission decrease in the order L-^{Me}Ar-OMe > L-^{Me}Ar-NHAc > L-Ar-NHAc, following the T_1 excited state energy (Table 1). Indeed, it seems that back-energy transfer from the Tb^{3+} $^5D_4$ state to the antenna T_1 state is responsible for this trend (the energy gap between antenna T_1 and Tb^{3+} $^5D_4$ states is particularly low for L-Ar-NHAc, *ca.* 1600 cm^{-1}), which is confirmed by longer lifetimes in deoxygenated PBS (ESI†). For all these compounds, comparison of Ln^{3+} luminescence lifetimes measured in H_2O and D_2O indicates that the hydration number q is zero, in agreement with the saturated coordination sphere expected for these ligands (ESI†).[27,34]

The 2P absorption cross-sections (σ_{2P}) in the NIR, between 680 and 800 nm, were determined for mTAT[Tb·L-^{Me}Ar-OMe], mTAT[Tb·L-^{Me}Ar-NHAc] and mTAT[Eu·L-Ar-NHAc] using the 2P excited fluorescence method (ESI†). For the three compounds, upon excitation at 720 nm, the characteristic Ln^{3+} emission is obtained and it displays a quadratic variation of intensity with respect to the incident laser power (Fig. 3A), the signature of a 2P-antenna effect. The 2P absorption spectrum was in good agreement with the wavelength-doubled 1P absorption one (Fig. 3B), indicating that the low-energy ILCT transition responsible for the sensitization of Ln^{3+} luminescence is one- and two-photon allowed. The values of σ_{2P} are low (Table 1), *ca.* 4–11 GM at 700 nm, and the compound with the freely rotating antenna, mTAT[Eu·L-Ar-NHAc], shows the highest cross-section. However, regarding the 2P brightness B_{2P} = $\sigma_{2P} \times \Phi_{Ln}$, which quantifies the efficiency of the whole absorption/emission process, mTAT[Tb·L-^{Me}Ar-OMe] appears to be the best compound with a B_{2P} value of 3.1 at 700 nm compared to 0.85 and 1.7 for mTAT[Tb·L-^{Me}Ar-NHAc] and mTAT[Eu·L-Ar-NHAc], respectively. In cells, the main contributors to 2P-excited autofluorescence are NAD(P)H and FAD.[37,38] They show emission bands with maxima at *ca.* 465 and 530 nm,[38] respectively, and quantum yields of *ca.* 0.02 and 0.03 at physiological pH, respectively.[39] Their 2P cross section under excitation around 700 nm is in the range 0.03–0.1 GM.[37] Their 2P brightness is therefore lower than that of the Ln^{3+}-based probes but the latter has to accumulate in sufficient amount in the cell to be detected efficiently, *i.e.* above the autofluorescence level.

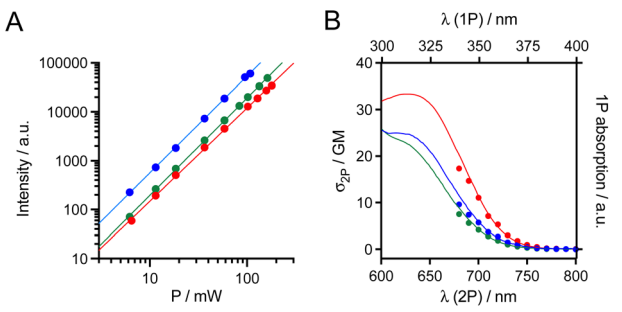

Fig. 3 (A) Quadratic power dependance of the Ln^{3+} emission (λ_{ex} = 680 nm) for mTAT[Tb·L-^{Me}Ar-OMe] (blue), mTAT[Tb L-^{Me}Ar-NHAc] (green) and mTAT[Eu·L-Ar-NHAc] (red) in PBS. Data sets were fitted using $I = A \times P^n$ yielding n = 1.91, 1.99 and 1.98, respectively. (B) Superimposition of 2P absorption spectra (lower abscissa for wavelength, dots) and 1P absorption spectra (upper abscissa, solid lines) for mTAT[Tb·L-^{Me}Ar-OMe] (blue), mTAT[Tb·L-^{Me}Ar-NHAc] (green) and mTAT[Eu·L-Ar-NHAc] (red) in PBS.

Given the better luminescence properties of mTAT [Tb·L-^{Me}Ar-OMe], mTAT[Tb·L-^{Me}Ar-NHAc] and mTAT[Eu·L-Ar-NHAc] compared to the other three compounds, we have synthesized and characterized their dimeric analogues dTAT [Tb·L-^{Me}Ar-OMe], dTAT[Tb·L-^{Me}Ar-NHAc] and dTAT[Eu·L-Ar-NHAc] (ESI† and Table 1). Dimeric dTAT[Eu·L-Ar-NHAc] and monomeric mTAT[Eu·L-Ar-NHAc] exhibit identical photophysical properties (Table 1). However, for the Tb^{3+} compounds, the luminescence quantum yields and lifetimes of the dimeric compounds are lower than their monomeric counterparts, probably due to additional deactivation by the T_1 state of the second Tb^{3+} complex of the dimer. However, should these compounds manage to reach the cell cytosol, the disulphide will be reduced due to its high glutathione content (*ca.* 4–5 mM).[40–42] Consequently, the monomeric form is likely to better represent the species present inside cells with associated photophysical properties.

Two-photon microscopy imaging of live cells

The cell imaging properties of the dTAT[Ln·L] conjugates were investigated by microscopy using 2P excitation at 720 nm. Live HeLa cells were incubated for 1 h with the dTAT[Ln·L] conjugates then washed and imaged. Images obtained with dTAT [Tb·L-^{Me}Ar-OMe] (10 μM) are shown in Fig. 4. In the DIC image (Fig. 4A, left), the cells phenotype is consistent with that of live cells. Luminescence emission under 2P excitation at 720 nm was collected with an avalanche photodiode (APD; Fig. 4A, middle panel) with a 420–650 nm bandpass (bp) filter. It was detected in all cells, but its intensity varied from cell to cell. Both punctate and diffuse emission signals are detected within cells, the latter covering in the entire cell. These features are reminiscent of the fluorescence pattern detected with dfTAT[32] and, more generally, are characteristic of fluorophores internalized with CPP. A single APD does not allow to identify the emissive species based on its emission spectrum. Therefore, spectral detection was performed using a photomultiplier (PMT array of Quasar detectors). The left panel of Fig. 4B shows the emission spectra averaged within the entire cell arising from the two cells outlined in red and green in panel 4A, left. These emission spectra are dominated by the Tb^{3+} emission but a weaker contribution from autofluorescence background is also detected. Deconvolution of the luminescence images

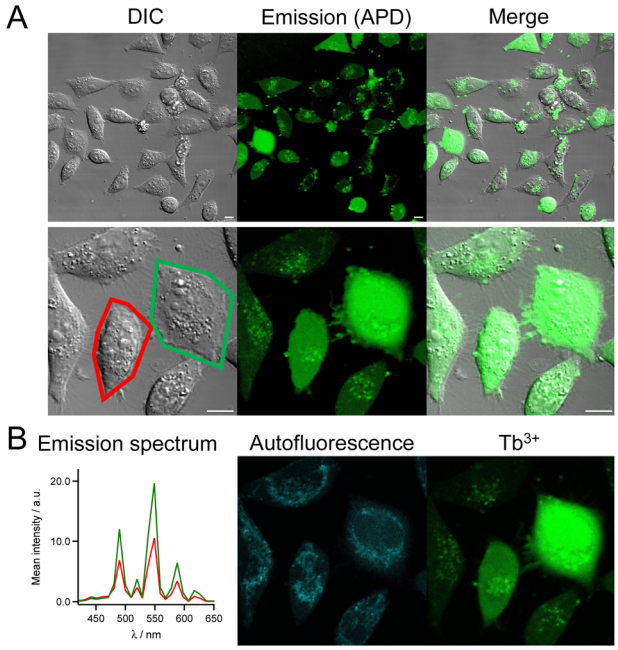

Fig. 4 2PM imaging (λ_{ex} = 720 nm) of living HeLa cells incubated 1 h with dTAT[Tb·L-^{Me}Ar-OMe] (10 μM) in RPMI medium. (A) Left panel: differential interference contrast (DIC) image; Middle panel: luminescence image recorded using a 420–650 nm bp filter and APD detection; Right panel: merge. Scale bars correspond to 10 μm. (B) Left panel: 2P-excited emission spectra (detected with PMT array) of cells outlined in red and green in panel A; Middle and right panels: autofluorescence and Tb^{3+} emission maps obtained by linear unmixing of 2P-excited spectral images recorded with the PMT.

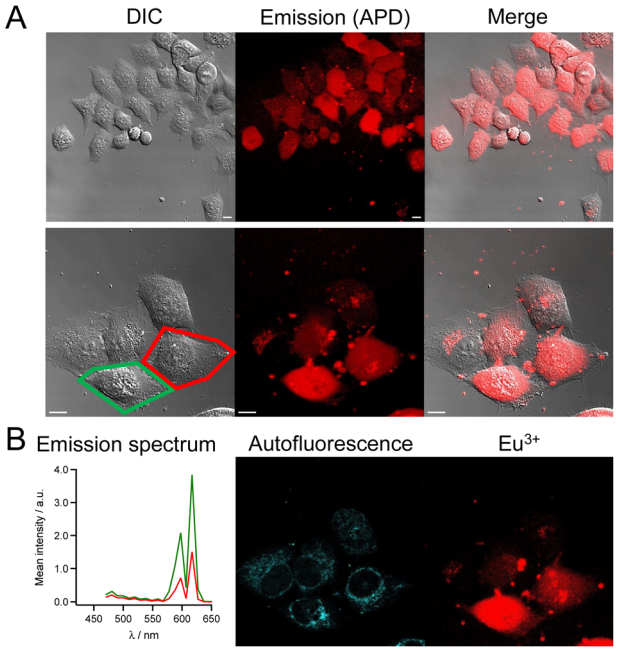

Fig. 5 2PM imaging (λ_{ex} = 720 nm) of living HeLa cells incubated 1 h with dTAT[Eu·L-Ar-NHAc] (10 μM) in RPMI medium. (A) Left panel: DIC image; Middle panel: luminescence image recorded using a 465–680 nm bp filter and APD detection; Right panel: merge. Scale bars correspond to 10 μm. (B) Left panel: 2P-excited emission spectra (detected with PMT array) of cells outlined in red and green in panel A; Middle and right panels: autofluorescence and Eu^{3+} emission maps obtained by linear unmixing of 2P-excited spectral images recorded with the PMT.

acquired in spectral mode resulted in the autofluorescence and Tb^{3+} emission maps showed in the middle and right panels of Fig. 4B, respectively. The autofluorescence localization is characteristic of the typical distribution of mitochondria, consistent with 2P excitation of NADH fluorescence. Tb^{3+} emission is detected in all cells, whether diffuse or punctate. The diffuse emission, which is observed in the entire cell, including nucleus, indicates successful cytosolic delivery of the Tb^{3+} complex, whereas the punctate emission may correspond to Tb^{3+} complexes still trapped in endosomes. After 4 h, the punctate distribution is still present. The luminescence decay of diffuse Tb^{3+} emission was measured in cells using TSLIM measurements[21] and could be fitted bi-exponentially with lifetimes of 0.75 and 0.15 ms (Fig. S12†), which are both shorter than the lifetime measured in PBS solution with a spectrometer (Table 1). Nevertheless, these millisecond values confirm emission arising from the Tb^{3+} ion.

Similar images and cell distributions were obtained with dTAT[Tb·L-^{Me}Ar-NHAc] (Fig. S13†) and dTAT[Eu·L-Ar-HNAc] after 1 h incubation at 10 μM (Fig. 5). In the former case, Tb^{3+} emission was clearly detected in cells by spectral detection although it was weaker than for dTAT[Tb·L-^{Me}Ar-OMe] compared to autofluorescence emission, consistent with the lower 2P brightness of the former. Nevertheless, the deconvolution of autofluorescence and Tb^{3+} emission (Fig. S13†) shows a Tb^{3+} signal that is both diffuse and punctate, with the diffuse component attesting to cytosolic delivery. A bi-exponential luminescence decay with lifetimes of 0.84 and 0.15 ms was measured in cells for the diffuse Tb^{3+} signal.

In the case of dTAT[Eu·L-Ar-HNAc], a large number of cells shows diffuse Eu^{3+} emission above the autofluorescence as shown in the spectrum in Fig. 5, with peaks at 590 and 615 nm. This confirms again the cytosolic delivery of the Eu^{3+} complex. Some cells show also punctate Eu^{3+} emission inside the cell but outside the nucleus, which may correspond to the Eu^{3+} probe trapped in endosomes or lysosomes. Small clumps of the Eu^{3+} probe are also observed in areas where no cell is present or sticked to the cell membrane. This may correspond to probe aggregates that form in the culture medium (not observed in drop of water solution of the probe, even at 100 μM). Within cells, the Eu^{3+} luminescence decay lifetime of diffuse emission was 0.65 ms. As for Tb^{3+} compounds, the lifetime measured in the living cell is shorter than in PBS solution. The lifetime measured in a drop of Ln^{3+} conjugate with the microscope is within margin error equal to the one determined in solution with a spectrometer, ruling out problems due to measurement procedure with the microscope. The reason is unclear but we can envisage that energy transfer from the excited Ln^{3+} to cell components (aromatic co-factors) happens. The reason of the bi-exponential decay of the Tb^{3+} needs further studies to be clarified.

Cell staining with dTAT[Eu·L-Ar-HNAc] was also studied in a concentration dependent manner. At 2.5 μM (1 h incubation),

cells only show punctate Eu^{3+} around the nucleus (Fig. S14†). Counter-staining with LysoView488™ (Biotium), a lysosome marker, shows excellent overlap with Eu^{3+} distribution (Fig. S15†), confirming that the punctate probe emission corresponds to endosomal/lysosomal entrapment. Next we examined the time dependence of the staining after 1 h incubation of HeLa cells with dTAT[Eu·L-Ar-HNAc] at 5 μM. The mean intensity of Eu^{3+} emission recorded using a 590–680 nm bp filter was measured within cells 20, 90, 240 and 360 min after washing (*ca.* 120 cells analysed at each time point) and compared to non-incubated HeLa cells as a control (Fig. 6A). The background emission was higher in incubated cells than in control, especially close to the surface. This may be attributed to dTAT[Eu·L-Ar-HNAc] adhered to the surface, as already described for CPP-rhodamine conjugates.[43] The distribution of mean intensity within cells does not vary significantly with time up to 6 h. The number of cells showing cytosolic staining, *i.e.* diffuse Eu^{3+} emission was also determined. It remains constant (34–38%) over 6 hours after washing (Fig. 6B). Punctate Eu^{3+} emission trapped in endosomes is still observed after 6 h in some cells.

Finally, internalization was confirmed in other cell types such as HEK293T or MRC5 cells with dTAT[Eu·L-Ar-HNAc] with successful cytosolic delivery demonstrated by the characteristic diffuse Eu^{3+} localization (Fig. 7). Interestingly, no significant internalization was observed with mTAT compounds in HeLa cells, demonstrating the importance of TAT dimerization for cell penetration efficiency and cytosolic delivery.

Cytotoxicity

The cytotoxicity of dTAT[Ln·L] conjugates was evaluated using the MTT proliferation assay. The compound concentration causing a 50% reduction in proliferation (IC_{50}) is given in Table 1 and plots of cell viability as a function of compound concentration are shown in Fig. 8 dTAT[Eu·L-Ar-HNAc] is the least toxic (IC_{50} > 50 μM), showing no toxicity at the 10 μM concentration used for 2PM. The IC_{50} of the two Tb^{3+} compounds carrying the *ortho*-methyl on the antenna are lower, with dTAT[Tb·L-^{Me}Ar-HNAc] being the most toxic with an IC_{50} below 10 μM. We also observed stronger toxicity (IC_{50} = 2.5 μM) with a related compound bearing a carbazole instead of a methoxy or acetamide electrodonating group (this compound will be described in detail elsewhere). Suspecting that the toxicity might be related to the hydrophobicity of the antenna and its possible interaction with membrane lipids, we synthesized two analogues of the more toxic Tb^{3+} compound but with charged pendants on the amide electrodonating group: dTAT[Tb·L-^{Me}Ar-NHβAla(+)] and dTAT[Tb·L-^{Me}Ar-NHSuc(−)] with an additional positive and negative charge, respectively. Their luminescence properties (Table 1) are similar to those of their parent compound dTAT[Tb·L-^{Me}Ar-NHAc], indicating that the introduction of the charge has little effect on the emission properties. Interestingly, however, the additional charge greatly reduces the toxicity (Table 1), increasing the IC_{50} values above 10 μM, which is the highest concentration used for 2P imaging experiments. It should be noted that the MTT assays were carried out with a 2 hour incubation instead of the 1 hour incubation for 2PM. Consequently, toxicity might be overestimated compared with 2PM conditions. 2PM imaging of HeLa cells showed that the additional charge does not alter the cell penetration properties: both dTAT[Tb·L-^{Me}Ar-NHβAla(+)] and dTAT[Tb·L-^{Me}Ar-NHSuc(−)] are efficiently delivered to the cytosol with characteristic diffuse emission (Fig. S16 and S17†). This demonstrates that the cytotoxicity of these compounds can be easily modulated by reducing the lipophilicity of the antenna, without affecting the photophysical, penetration and imaging properties.

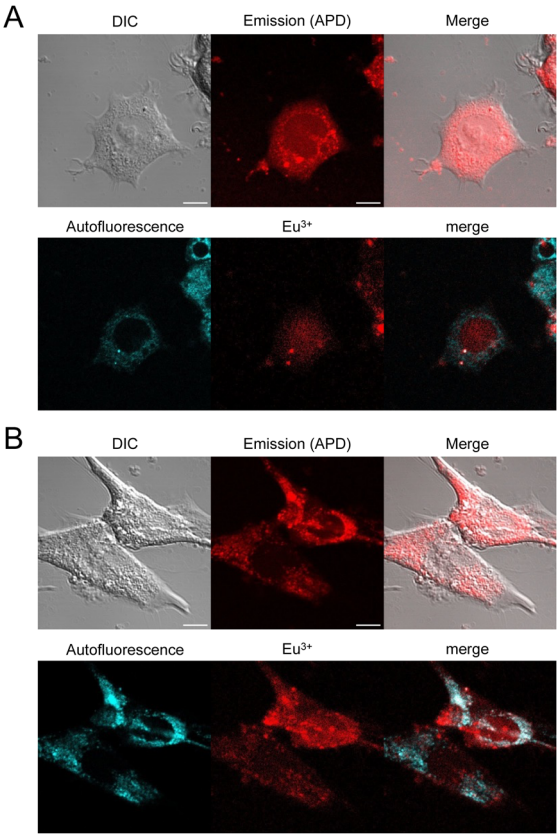

Fig. 7 2PM imaging (λ_{ex} = 720 nm) of living HEK293T (A) and MRC5 (B) cells incubated 1 h with dTAT[Eu·L-Ar-NHAc] (10 μM) in RPMI medium. Top: DIC, emission recorded using using a 465–680 nm bp filter and merge; Bottom: linear unmixing of autofluorescence (AF) and Eu^{3+} emission and merge. Scale bars correspond to 10 μm.

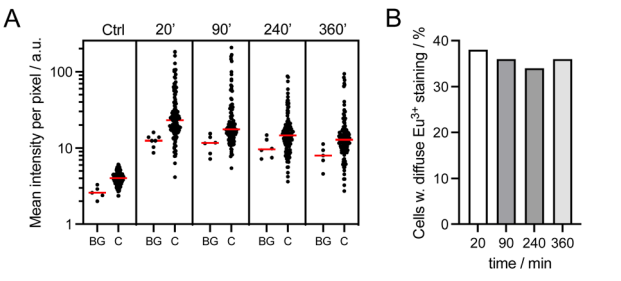

Fig. 6 Time dependence of cell staining with dTAT[Eu·L-Ar-NHAc] (5 μM, 1 h). (A) Mean emission intensity measured in the red (590–680 bp filter) for background (BG) and within cells (C); median value is shown in the red. (B) Percentage of cells showing diffuse Eu^{3+} staining, as determined visually.

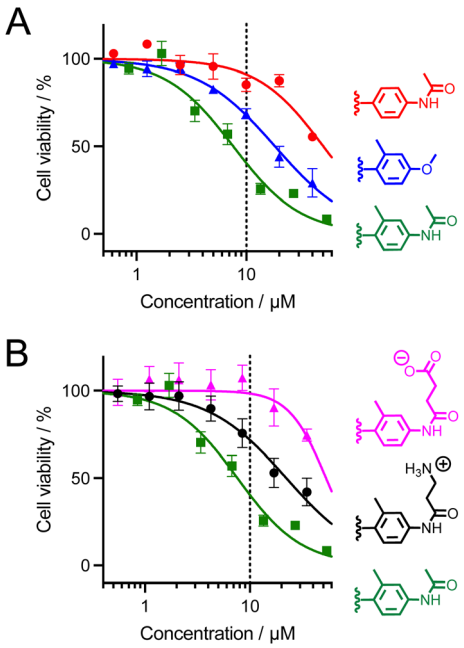

Fig. 8 MTT proliferation assay for dTAT[Ln·L] conjugates. (A) Red: dTAT[Eu·L-Ar-NHAc]; blue: dTAT[Tb·L-^{Me}Ar-OMe]; green: dTAT[Tb·L-^{Me}Ar-NHAc]. (B) Pink: dTAT[Tb·L-^{Me}Ar-NHSuc(−)]; black: dTAT[Tb·L-^{Me}Ar-NHβAla(+)]; green: dTAT[Tb·L-^{Me}Ar-NHAc]. Symbols correspond to experimental data and solid lines to the fit that yielded IC_{50} values given in Table 1. Error bars correspond to the SEM. The dotted line indicates the highest concentration used for 2P microscopy in this article (10 μM).

Toward multiplex imaging

Finally, since these compounds have similar 2P brightness, we attempted cell imaging with a Tb^{3+}/Eu^{3+} mixture. HeLa cells were incubated for 1 h with dTAT[Tb·L-^{Me}Ar-NHβAla(+)] (10 μM) and dTAT[Eu·L-Ar-NHAc] (5 μM), rinsed and imaged by 2P microscopy. A luminescence emission could be detected within the cells, the intensity of which again varied from cell to cell (Fig. 9). However, the diffuse emission was detected in many cells. The emission spectrum arising from cells under 2P excitation at 720 nm clearly shows fingerprint peaks of Tb^{3+} (490 and 540 nm) and Eu^{3+} (590 and 615 nm) emission (Fig. 9B). This indicates that both Tb^{3+} and Eu^{3+} complexes were co-internalized in the cells. Spectral deconvolution (Fig. 9B, right) showed that they were delivered to the cytosol because of the diffuse signal and co-localized well throughout the entire cell. A similar Tb^{3+}/Eu^{3+} co-internalization could be obtained with dTAT[Tb·L-^{Me}Ar-NHSuc(−)] (Fig. S18†). This opens the way to multiplex imaging with multiple Ln^{3+} probes in living cells.

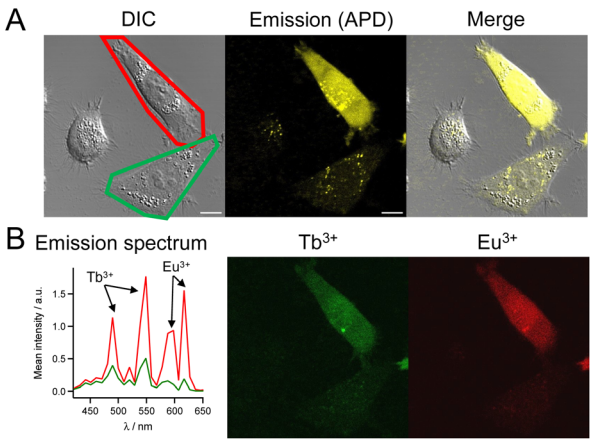

Fig. 9 2PM imaging (λ_{ex} = 720 nm) of living HeLa cells incubated 1 h with dTAT[Tb·L-^{Me}Ar-NHβAla(+)] (10 μM) and dTAT[Eu·L-Ar-NHAc] (3 μM) in RPMI medium. (A) Left panel: DIC image; Middle panel: luminescence image recorded using APD; Right panel: merge. Scale bars correspond to 10 μm. (B) Left panel: 2P-excited emission spectra (detection with PMT array) of cells outlined in red and green in panel A; Middle and right panels: Tb^{3+} and Eu^{3+} emission maps obtained by linear unmixing of 2P-excited spectral images recorded with the PMT.

Conclusion

In the present work we report a family of luminescent lanthanide bioprobes, named dTAT[Ln·L], that are efficiently delivered into the cytosol of living cells and allow two-photon microscopy imaging. These probes are based on a TAT dimer functionalized by Ln^{3+} complexes, which exhibit 2P absorption properties thanks to a push–pull antenna. As a Ln^{3+} chelator (L), we choose DO3Apic but equipped with different π-extended picolinate moieties. It can be easily conjugated to peptides *via* the picolinate group and forms stable Tb^{3+} and Eu^{3+} complexes with good to excellent photophysical properties. Optical properties identified three candidates for 2PM imaging of cells, *i.e.* two Tb^{3+} and one Eu^{3+} complexes with quantum yields ≥15% and featuring 2P absorption. 2PM of live HeLa cells incubated for 1 h with these complexes conjugated to TAT dimers showed intense Ln^{3+} emission under 2P excitation at 720 nm despite their low 2P cross sections. Successful cytosolic delivery of the Ln^{3+} complex was observed in most cells with characteristic diffuse Tb^{3+} or Eu^{3+} emission within the entire cell. The conjugates can be used to image other cell types as demonstrated with HEK293T and MRC5 cells. Interestingly, we have shown that the potential toxicity of these conjugates can be easily reduced to acceptable levels by adding charges onto the antenna to reduce its lipophilicity. In contrast to the dimeric dTAT[Ln·L] compounds, the monomeric analogues mTAT[Ln·L] are unable to penetrate cells sufficiently for 2PM imaging. Hence, this article shows that the TAT dimer is a suitable scaffold for the design of Ln^{3+}-based luminescent probes that have to be delivered into the cytosol of living cells.

The controlled delivery of dTAT[Ln·L] is really innovative compared to previous Ln^{3+} luminescent probes that required cell fixation to permeabilize the cell membranes for probe internalization or that accumulated in an uncontrolled manner in either lysosomes or mitochondria of living cells. Importantly, 2PM imaging with the dTAT[Ln·L] conjugates was performed using a commercial confocal microscope routinely used in biology laboratories and Ln^{3+} could be fully characterized inside cells by recording the emission spectrum and the millisecond luminescence decay lifetime.

Finally, given the design of these probes and the versatility offered by their synthetic pathway, there is room to improve their photophysical properties. The design described here

opens the way to more sophisticated responsive probes with ratiometric detection based on emission intensity using mixtures of Ln^{3+} or emission lifetime.

Data availability

The datasets supporting this article have been uploaded as part of the ESI.† They are also available from the authors on reasonable request.

Author contributions

Conceptualization: O. S., O. M.; investigation: K. P. M., T. C., D. N., J.-H. C., L. B., B. C., G. M., S. E., V. M.-F., A. G., O. S.; validation: O. S., A. B., O. M., V. M.-F., A. G.; witting (original draft): O. S.; writing (review & editing): all authors. Visualization: O. S.

Conflicts of interest

There are no conflicts to declare.

Acknowledgements

Authors acknowledge the Labex ARCANE, CBH-EUR-GS (ANR-17-EURE-0003), the Agence Nationale de la Recherche (ANR-18-CE06-0022), the CEA FOCUS Biomarqueurs program and the Aviesan ITMO Cancer PCSI program (ONCOVIEW project) for financial support. Imaging experiments were done on Microcell core facility of the Institute for Advanced Biosciences (UGA - Inserm U1209 - CNRS 5309). This facility belongs to the IBISA-ISdV platform, member of the national infrastructure France-BioImaging supported by the French National Research Agency (ANR-10-INBS-04).

Notes and references

1 E. Haustein and P. Schwille, *HFSP J.*, 2007, **1**, 169–180.
2 K.-J. Halbhuber and K. König, *Ann. Anat.*, 2003, **185**, 1–20.
3 A. D. Elliott, *Curr. Protoc. Cytom.*, 2020, **92**, e68.
4 T. Ueno and T. Nagano, *Nat. Methods*, 2011, **8**, 642–645.
5 L. D. Lavis and R. T. Raines, *ACS Chem. Biol.*, 2008, **3**, 142–155.
6 M. Wang, Y. Da and Y. Tian, *Chem. Soc. Rev.*, 2023, **52**, 1189–1214.
7 W. Denk, J. H. Strickler and W. W. Webb, *Science*, 1990, **248**, 73–76.
8 R. J. Gillies, *J. Cell. Biochem.*, 2002, 231–238.
9 J. B. Grimm, B. P. English, J. Chen, J. P. Slaughter, Z. Zhang, A. Revyakin, R. Patel, J. J. Macklin, D. Normanno, R. H. Singer, T. Lionnet and L. D. Lavis, *Nat. Methods*, 2015, **12**, 244–250.
10 C. Ding and T. Ren, *Coord. Chem. Rev.*, 2023, **482**, 215080.
11 L. Xu, J. Zhang, L. Yin, X. Long, W. Zhang and Q. Zhang, *J. Mater. Chem. C*, 2020, **8**, 6342–6349.
12 J.-C. G. Bünzli and S. V. Eliseeva, in *Lanthanide Luminescence*, ed. P. Hänninen and H. Härmä, Springer Berlin Heidelberg, 2011, pp. 1–45.
13 J.-C. G. Bünzli, *J. Lumin.*, 2016, **170**, 866–878.
14 M. Sy, A. Nonat, N. Hildebrandt and L. J. Charbonnière, *Chem. Commun.*, 2016, **52**, 5080–5095.
15 E. Mathieu, A. Sipos, E. Demeyere, D. Phipps, D. Sakaveli and K. E. Borbas, *Chem. Commun.*, 2018, **54**, 10021–10035.
16 G.-Q. Jin, Y. Ning, J.-X. Geng, Z.-F. Jiang, Y. Wang and J.-L. Zhang, *Inorg. Chem. Front.*, 2020, **7**, 289–299.
17 D. Parker, J. D. Fradgley and K.-L. Wong, *Chem. Soc. Rev.*, 2021, **50**, 8193–8213.
18 A. Picot, A. D'Aleo, P. L. Baldeck, A. Grichine, A. Duperray, C. Andraud and O. Maury, *J. Am. Chem. Soc.*, 2008, **130**, 1532–1533.
19 A. D'Aléo, A. Bourdolle, S. Brustlein, T. Fauquier, A. Grichine, A. Duperray, P. L. Baldeck, C. Andraud, S. Brasselet and O. Maury, *Angew. Chem., Int. Ed.*, 2012, **51**, 6622–6625.
20 N. Hamon, A. Roux, M. Beyler, J.-C. Mulatier, C. Andraud, C. Nguyen, M. Maynadier, N. Bettache, A. Duperray, A. Grichine, S. Brasselet, M. Gary-Bobo, O. Maury and R. Tripier, *J. Am. Chem. Soc.*, 2020, **142**, 10184–10197.
21 A. Grichine, A. Haefele, S. Pascal, A. Duperray, R. Michel, C. Andraud and O. Maury, *Chem. Sci.*, 2014, **5**, 3475–3485.
22 R. A. Poole, C. P. Montgomery, E. J. New, A. Congreve, D. Parker and M. Botta, *Org. Biomol. Chem.*, 2007, **5**, 2055–2062.
23 R. Pal and D. Parker, *Org. Biomol. Chem.*, 2008, **6**, 1020–1033.
24 C. P. Montgomery, B. S. Murray, E. J. New, R. Pal and D. Parker, *Acc. Chem. Res.*, 2009, **42**, 925–937.
25 E. J. New and D. Parker, *Org. Biomol. Chem.*, 2009, **7**, 851–855.
26 E. J. New, A. Congreve and D. Parker, *Chem. Sci.*, 2010, **1**, 111–118.
27 J.-H. Choi, G. Fremy, T. Charnay, N. Fayad, J. Pécaut, S. Erbek, N. Hildebrandt, V. Martel-Frachet, A. Grichine and O. Sénèque, *Inorg. Chem.*, 2022, **61**, 20674–20689.
28 C. P. Montgomery, D. Parker and L. Lamarque, *Chem. Commun.*, 2007, 3841–3843.
29 S. J. Butler, L. Lamarque, R. Pal and D. Parker, *Chem. Sci.*, 2014, **5**, 1750–1756.
30 L. Peraro and J. A. Kritzer, *Angew. Chem., Int. Ed.*, 2018, **57**, 11868–11881.
31 F. Nadal-Bufí and S. T. Henriques, *Pept. Sci.*, 2020, **112**, e24168.
32 A. Erazo-Oliveras, K. Najjar, L. Dayani, T.-Y. Wang, G. A. Johnson and J.-P. Pellois, *Nat. Methods*, 2014, **11**, 861–867.
33 J. K. Allen, D. J. Brock, H. M. Kondow-McConaghy and J.-P. Pellois, *Biomolecules*, 2018, **8**, 50.
34 M. Regueiro-Figueroa, B. Bensenane, E. Ruscsak, D. Esteban-Gomez, L. J. Charbonniere, G. Tircso, I. Toth, A. de Blas, T. Rodriguez-Blas and C. Platas-Iglesias, *Inorg. Chem.*, 2011, **50**, 4125–4141.
35 A. D'Aléo, M. Allali, A. Picot, P. L. Baldeck, L. Toupet, C. Andraud and O. Maury, *C. R. Chim.*, 2010, **13**, 681–690.

36 A. T. Bui, A. Roux, A. Grichine, A. Duperray, C. Andraud and O. Maury, *Chem.–Eur. J.*, 2018, **24**, 3408–3412.
37 Y. Qin and Y. Xia, *Front. Phys.*, 2021, **9**, 642302.
38 R. Cao, H. K. Wallrabe and A. Periasamy, *J. Biomed. Opt.*, 2020, **25**, 014510.
39 I. A. Gorbunova, M. K. Danilova, M. E. Sasin, V. P. Belik, D. P. Golyshev and O. S. Vasyutinskii, *J. Photochem. Photobiol., A*, 2023, **436**, 114388.
40 R. C. Cumming, N. L. Andon, P. A. Haynes, M. Park, W. H. Fischer and D. Schubert, *J. Biol. Chem.*, 2004, **279**, 21749–21758.
41 C. D. Austin, X. Wen, L. Gazzard, C. Nelson, R. H. Scheller and S. J. Scales, *Proc. Natl. Acad. Sci. U. S. A.*, 2005, **102**, 17987–17992.
42 Y.-J. Lee, S. Datta and J.-P. Pellois, *J. Am. Chem. Soc.*, 2008, **130**, 2398–2399.
43 M. Serulla, P. Anees, A. Hallaj, E. Trofimenko, T. Kalia, Y. Krishnan and C. Widmann, *Eur. J. Pharm. Biopharm.*, 2023, **184**, 116–124.

Efficient Cytosolic Delivery of Luminescent Lanthanide Bioprobes in Live Cells for Two-Photon Microscopy

Kyangwi P. Malikidogo,[a,b,+,#] Thibault Charnay,[a,b,+] Daouda Ndiaye,[a] Ji-Hyung Choi,[a] Lucile Bridou,[c] Baptiste Chartier,[a] Sule Erbek,[d,e] Guillaume Micouin,[c] Akos Banyasz,[c] Olivier Maury,[f] Véronique Martel-Frachet,[d,e] Alexei Grichine[d] and Olivier Sénèque*[a]

[a] Univ. Grenoble Alpes, CNRS, CEA, IRIG, LCBM (UMR 5249), F-38000 Grenoble, France.

[b] Univ. Grenoble Alpes, CNRS, DCM (UMR 5250), F-38000 Grenoble, France.

[c] Univ Lyon, ENS de Lyon, CNRS UMR 5182, Laboratoire de Chimie, Lyon F-69342, France.

[d] Univ. Grenoble Alpes, INSERM U1209, CNRS UMR 5309, Institute for Advanced Biosciences, F-38000 Grenoble, France.

[e] EPHE, PSL Research University, 4-14 rue Ferrus, 75014 Paris, France.

[+] These authors contributed equally to this work.

[#] Present address: Faculté des Sciences et Technologies, Université de Goma, B.P. 204 Goma, R. D. Congo.

Email: *olivier.seneque@cea.fr*

Supporting Information

Content

Abbreviations

Alloc: allyloxycarbonyl; aq.: aqueous; Boc: *tert*-butyloxycarbonyl; DCC: dicyclohexylcarbodimide; DIEA: *N*,*N*-diisopropyl-ethylamine; DMAP: *N*,*N*-dimethylaminopyridine; dppf: 1,1'-*bis*(diphenylphosphino)ferrocene; EDTA, ethylenediamine-tetraacetic acid; ESI: electrospray ionization; Fmoc: 9-fluorenyl-methoxycarbonyl; HCTU: *O*-(1*H*-6-chlorobenzotriazole-1-yl)-1,1,3,3-tetramethyluronium hexafluorophosphate; HEPES: 2-(4-(2-hydroxyethyl)piperazin-1-yl)ethanesulfonic acid; HRMS: high resolution mass spectrometry; LRMS: low resolution mass spectrometry; MTT: 3-(4,5-dimethylthiazol-2-yl)-2,5-diphenyltetrazolium bromide ; NMP: *N*-methyl-2-pyrrolidone; Pbf: 2,2,4,6,7-pentameethyldihydrobenzofuran-5-sulfonyl; PyBOP: (benzotriazol-1-yloxy)tripyrrolidinophosphonium hexafluorophosphate; SPPS: solid-phase peptide synthesis; TIS: triisopropylsilane; Trt: trityl.

Materials and methods

Reagents and solvents: N-α-Fmoc-protected amino acids for peptide synthesis, HCTU and PyBOP coupling reagent and NovaPEG Rink Amide resin were purchased from Novabiochem or Iris Biotech. Other reagents for peptide synthesis, solvents, buffers and metal salts were purchased from Sigma-Aldrich. All buffer or metal solutions for spectroscopic measurements were prepared with ultrapure water produced by a Millipore Milli-Q purification system (purified to 18.2 MΩ.cm). Buffer solutions were treated with Chelex 100 resin (Bio-Rad) to remove trace metal ions.

HPLC purifications: Analytical HPLC/LRMS analyses were performed on an Agilent Infinity 1260 II system equipped with a 6125 MS (ESI) detector using a Waters XBridge BEH130 C18 (2.5 µm, 75 mm × 4.6 mm). Preparative HPLC separations were performed on a VWR LaPrepΣ system using Waters XBridge Peptide BEH130 C18 (5 µm, 150 mm × 19 mm) or Waters XBridge Peptide BEH130 C18 (5 µm, 150 mm × 10 mm) columns at flow rates of 14 or 6 mL/min, respectively. Mobile phase consisted in a gradient of solvent A (0.1 % TFA in H_2O) and B (0.1 % TFA in MeCN/H_2O 9:1). For analytical separations, Method B consisted in 5% B during 1 min followed by a 5 to 100 % B gradient in 13 min at 1 mL/min. Eluate was monitored by electronic absorption at 214, 280 and 331 nm as well as by LRMS (ESI+) detection.

NMR spectroscopy: ^{1}H, ^{13}C and DEPT NMR spectra were recorded at 400 MHz on a Varian Avance III 400 spectrometer at 298 K unless specified. Coupling constants (*J*) are measured in Hertz and are given with 0.5 Hz accuracy and the chemical shift (δ) are measured in ppm. All chemical shifts for ^{1}H and ^{13}C spectra were referenced to the residual solvent peak ($CDCl_3$ δ_H = 7.26 ppm and δ_C = 77.2 ppm; CD_3OD δ_H = 3.31 ppm and δ_C = 49.0 ppm). The following abbreviations were for peak multiplicities: s (singlet), d (doublet), t (triplet), m (multiplet), br (broad peak(s)).

Mass spectrometry: LRMS(ESI) analyses were performed on a Thermo Scientific LXQ spectrometer. HRMS (ESI) were performed on a Thermo Scientific LTQ Orbitrap XL spectrometer or on a Waters Xevo G2-S QTof spectrometer with electrospray ionization.

Optical spectroscopy: UV-Vis absorption spectra were recorded on a Perkin-Elmer Lambda 35 spectrophotometer or on a Varian Cary 50 spectrometer, both equipped with a thermo-regulated cell holder. Luminescence spectra were measured on a Varian Cary Eclipse spectrometer equipped with a thermo-regulated cell holder or on a modular Fluorolog FL3-22 spectrometer from Horiba-Jobin Yvon-Spex equipped with a double-grating excitation monochromator and an iHR320 imaging spectrometer coupled to Hamamatsu R928P and Hamamatsu R5509 photomultipliers for visible and NIR detection, respectively. Emission spectra were corrected for wavelength-dependent detector response. Time-gated Ln^{3+} luminescence spectra were acquired with 100 µs time delay and 2 ms gate time on the Varian Cary Eclipse spectrometer. Ln^{3+} luminescence lifetimes were measured using the Varian Cary Eclipse spectrometer.

Synthesis

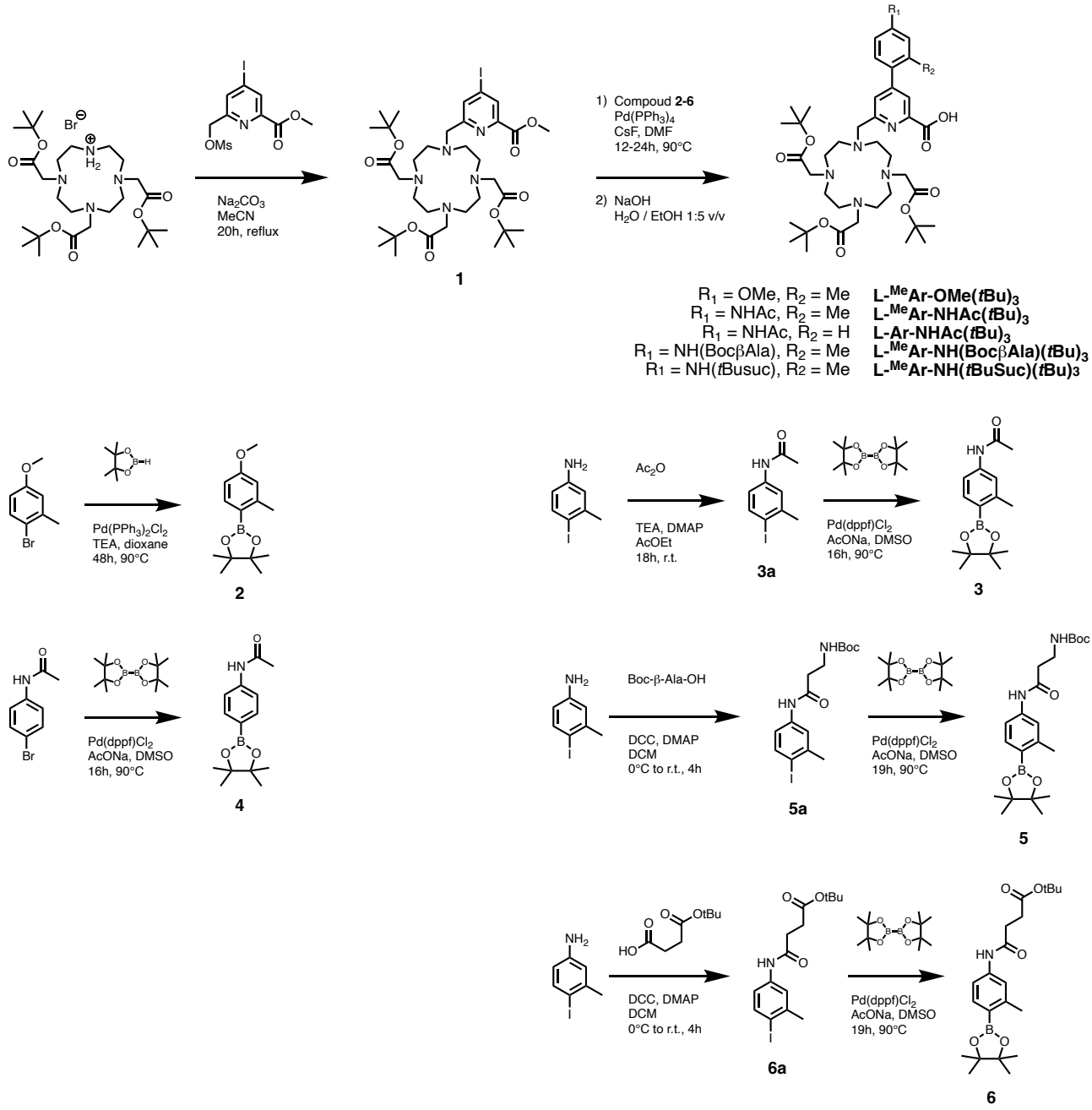

Fig. S1 Synthetic pathways for pro-ligands L(tBu)$_3$.

Compound 1: Na_2CO_3 (1.58 g, 15.0 mmol) was added to a solution of [1,4,7-*tris*(*tert*-butoxycarbonylmethyl)]-1,4,7,10-tetraazacyclododecane hydrobromide[1] (1.8 g, 3.0 mmol) in MeCN (10 mL). Then a solution of methyl 4-iodo-6-(((methylsulfonyl)oxy)methyl)picolinate[2] (1.1 g, 3.0 mmol) in MeCN (10 mL) was added. The mixture was heated at reflux for 20 h, then cooled to room temperature and filtrated over Celite. The solvent was evaporated under reduced pressure and the residue was triturated in AcOEt and sonicated to give **1** as a white powder (1.92 g, 82 %). ^{1}H NMR (400 MHz, $CDCl_3$): δ = 8.32 (d, J = 1.5, 1H), 7.96 (d, J = 1.5, 1H), 3.90 (s, 3H), 3.76 (br, 2H), 3.40-2.20, (m, 22H), 1.46 (s, 9H), 1.34 (s, 18H); ^{13}C{^{1}H} NMR (100 MHz, $CDCl_3$): δ = 172.4, 171.6, 164.1, 160.1, 147.0, 136.2, 132.9, 107.5, 82.3, 82.1, 58.8, 56.3, 56.1, 53.2, 50.7, 28.1, 28.0; LRMS (ESI+): monoisotopic *m/z* = 790.3 (+) / calculated *m/z* = 790.3 $[M+H]^+$ for M = $C_{34}H_{56}N_5O_8I$; HRMS (ESI+): monoisotopic *m/z* = 790.3239 (+) / calculated *m/z* = 790.3246 $[M+H]^+$ for M = $C_{34}H_{56}N_5O_8I$.

4-(4,4,5,5-tetramethyl-1,3,2-dioxaborolan-2-yl)-3-methylanisole 2: To a solution of 4-bromo-3-methylanisole (157 µL, 1.1 mmol) and 4,4,5,5-tetramethyl-1,3,2-dioxa-borolane (260 µL, 1.8 mmol) in dry dioxane (15 mL) were added *bis*(triphenylphosphine)palladium(II) dichloride (25 mg, 0.03 mmol) and triethylamine (500 µL, 3.6 mmol). The reaction was stirred at 90°C under argon for 48 h, then cooled to room temperature and filtrated over Celite. The solvent was removed under reduced pressure and the solid obtained was dissolved in DCM. The organic phase was washed with water twice. The organic layer was dried over Na_2SO_4 and the solvent was removed under reduced pressure. The crude product was purified by flash chromatography (silica gel, Cyclohexane/DCM 1:1) to give a white powder (195 mg, 88 %). ^{1}H NMR (400 MHz, $CDCl_3$): δ = 7.72 (d, J = 8.5, 1H), 6.71 (m, 2H), 3.81 (s, 3H), 2.53 (s, 3H), 1.33 (s, 12H); ^{13}C{^{1}H} NMR (100 MHz, $CDCl_3$): δ = 161.8, 147.4, 138.0, 115.7, 110.3, 83.3, 55.1, 25.0, 22.5. Spectroscopic data corresponded to literature.[3]

L-^{Me}Ar-OMe(tBu)$_3$: Compound **2** (61 mg, 0.25 mmol) and compound **1** (147 mg, 0.19 mmol) were dissolved in anhydrous DMF (5 mL). Cesium fluoride (109 mg, 0.72 mmol) and *tetrakis*(triphenylphosphine)palladium(0) (28 mg, 0.025 mmol, 0.1 eq.) were added. The reaction was stirred at 90 °C for 24 h. The reaction mixture was cooled to room temperature and the solvent was removed under reduced pressure. The residue was dissolved in DCM and the solution was washed with water. The organic layer was dried over Na_2SO_4 and the solvent was evaporated. The crude product was dissolved in EtOH (20 mL). NaOH 6 M (4 mL) was added dropwise and the reaction mixture was stirred for 20 min. The solution was neutralized using saturated $NaHCO_3$. After extraction with AcOEt, the organic layer was washed with water and dried over Na_2SO_4. The solvent was removed under reduced pressure. The crude product was purified by HPLC to give a yellow powder (98 mg, 46 % calculated based of the formula **L-^{Me}Ar-OMe(tBu)$_3$·3TFA**). HPLC (anal.): t_R = 10.9 min (method B); ^{1}H NMR (400 MHz, $CDCl_3$): δ = 8.12 (s, 1H), 7.50 (s, 1H), 7.15 (d, J = 9.0, 1H), 6.82 (m, 2H), 4.51 (s, 2H), 3.88 (s, 2H), 3.84 (s, 3H), 3.7–3.1 (m, 20H), 2.28 (s, 3H) 1.43 (s, 9H), 1.38 (s, 18H); ^{13}C{^{1}H} NMR (100 MHz, $CDCl_3$): δ = 168.3, 167.3, 166.0 161.2 (q, J = 37, TFA), 160.4, 153.2, 148.0, 136.8, 131.0, 129.8, 127.4, 125.8, 116.6, 116.3 (q, J = 291, TFA), 112.1, 84.3, 83.6, 57.6, 55.5, 55.3, 54.6, 50.9, 50.6, 49.5, 28,1, 28.0, 20.7; LRMS (ESI+): monoisotopic *m/z* = 770.7 (+), 792.7 (+) / calculated *m/z* = 770.5 $[M+H]^+$, 792.7 $[M+Na]^+$, for M = $C_{41}H_{63}N_5O_9$; HRMS (ESI+): monoisotopic *m/z* = 770.4703 (+) / calculated *m/z* = 770.4699 $[M+H]^+$ for M = $C_{41}H_{63}N_5O_9$.

4-(4,4,5,5-tetramethyl-1,3,2-dioxaborolan-2-yl)-3-methylacetanilide (3): Compound **3a**[4] (300 mg, 1.1 mmol), bis(pinacolato)diboron (305 mg, 1.2 mmol), [1,1'-*bis*(diphenylphosphino)ferrocene]palladium(II) dichloride (40 mg, 0.05 mmol) and sodium acetate (214 mg, 2.2 mmol) were dissolved in dried DMSO (2 mL). The solution was degassed using argon during 30 min. The reaction was stirred at 90 °C under argon for 16 h. The reaction mixture was cooled to room temperature then it was diluted in AcOEt and filtrated over Celite. The organic layer was washed with saturated NH_4Cl twice and then with water. The organic layer was dried over Na_2SO_4 and the solvent was removed under reduced pressure. The crude product was purified by flash chromatography (silica gel, DCM/MeOH 98:2) to give a colourless oil (275 mg, 91 %).^{1}H NMR (400 MHz, $CDCl_3$): δ = 7.71 (d, J = 8.0, 1H), 7.33 (s, 1H), 7.29 (d, J = 8.0, 1H), 2.52 (s, 3H), 2.16 (s, 3H), 1.33 (s, 12H); ^{13}C{^{1}H} NMR (100 MHz, $CDCl_3$): δ = 168.4, 146.6, 140.3, 137.3, 120.5, 115.8, 83.6, 53.7, 25.0, 22.5; LRMS (ESI+): monoisotopic m/z = 276.2 (+) / calculated *m/z* = 276.2 $[M+H]^+$, for M = $C_{15}H_{23}NO_3B$.

L-^{Me}Ar-NHAc(tBu)$_3$: Compound **3b** (60 mg, 0.23 mmol), compound **1** (160 mg, 0.2 mmol), cesium fluoride (90 mg, 0.59 mmol) and *tetrakis*(triphenylphosphine)palladium(0) (20 mg, 0.02 mmol) were dissolved in anhydrous DMF (2.5 mL). The reaction was stirred during 12 h at 90 °C under argon. The reaction mixture was cooled to room temperature and it was diluted using AcOEt. The solution was washed with saturated $NaHCO_3$ then water. The organic layer was dried over Na_2SO_4 and the solvent was removed under reduced pressure. The crude product was dissolved in EtOH (20 mL). NaOH 6 M (4 mL) was added dropwise and the reaction mixture was stirred for 10 min at room temperature. The solution was neutralized by dropwise addition of HCl 6 M (*ca.* 4 mL) and a precipitate was formed. The suspension was centrifugated and AcOEt was added to the supernatant. The organic layer was washed with water, dried over Na_2SO_4 and

the solvent was removed under reduced pressure. The product obtained was purified by HPLC to give a white powder (84 mg, 38 % calculated based of the formula **L-^{Me}Ar-NHAc (*t*Bu)$_3$·3TFA**). HPLC (anal.): t_R = 9.7 min (method B); ^{1}H NMR (400 MHz, CD_3OD): δ = 8.15 (s, 1H), 7.72 (d, J = 1.0, 1H), 7.57 (m, 2H), 7.24 (d, J = 8.0, 1H), 4.66 (s, 2H), 3.99-3.12 (br, 22H), 2.34 (s, 3H), 2.15 (s, 3H), 1.49 (s, 9H), 1.34 (s, 18H); $^{13}C\{^1H\}$ NMR (100 MHz, CD_3OD): δ = 171.9, 167.4, 162.5 (q, J = 38, TFA), 153.3, 149.0, 141.0, 137.1, 134.3, 131.2, 129.4, 126.8, 123.1, 119.5, 119.0, 118.2 (q, J = 291, TFA), 85.4, 84.0, 58.1, 56.0, 55.2, 52.2, 50.7, 28.4, 23.9, 20.8; LRMS (ESI+): monoisotopic *m/z* = 797.5 (+) / calculated *m/z* = 797.5 $[M+H]^+$, for M = $C_{42}H_{64}N_6O_9$; HRMS (ESI+): monoisotopic *m/z* = 797.4809 (+) / calculated *m/z* = 797.4808 $[M+H]^+$ for M = $C_{42}H_{64}N_6O_9$.

(4-(4,4,5,5-tetramethyl-1,3,2-dioxaborolan-2-yl)acetanilide (4): 4-bromoacetanilide (300 mg, 1.4 mmol), bis(pinacolato)diboron (391 mg, 1.5 mmol), [1,1'-*bis*(diphenylphosphino)ferrocene]palladium(II) dichloride (102 mg, 0.1 mmol) and sodium acetate (275 mg, 2.8 mmol) were dissolved in DMSO (2 mL). The solution was degassed using argon during 30 min. The reaction was stirred during 24 h at 90 °C under argon. The reaction mixture was diluted in AcOEt. The organic layer was washed with saturated NaCl then water and dried over Na_2SO_4. The solvent was removed under reduced pressure. The crude product was purified by flash chromatography (silica gel, AcOEt/Cyclohexane 30:70) to give a yellow oil (284 mg, 78 %). ^{1}H NMR (400 MHz, $CDCl_3$): δ = 7.76 (d, J = 8.5, 2H), 7.50 (d, J = 8.5, 2H), 7.16 (s, 1H), 2.19 (s, 3H), 1.35 (s, 12H); $^{13}C\{^1H\}$ NMR (100 MHz, $CDCl_3$): δ = 168.4, 140.6, 136.0, 118.6, 83.9, 29.9, 25.0. Spectroscopic data correspond to literature.[5]

L-Ar-NHAc(*t*Bu)$_3$: Compound **4** (68 mg, 0.26 mmol), compound **1** (133 mg, 0.17 mmol), cesium fluoride (83 mg, 0.55 mmol) and *tetrakis*(triphenylphosphine)palladium(0), polymer-bound (25 mg, 0.01 mmol) were dissolved in anhydrous DMF (2.5 mL). The reaction was stirred at 90 °C under argon for 24 h. The reaction mixture was cooled to room temperature and filtered over Celite. The solvent was removed under reduced pressure. The residue was dissolved in AcOEt. The organic phase was washed with saturated $NaHCO_3$ then water and dried over Na_2SO_4. The solvent was removed under reduced pressure. The crude product was dissolved in EtOH (20 mL). NaOH 6 M (4 mL) was added dropwise and the reaction mixture was stirred for 10 min at room temperature. The solution was neutralized by dropwise addition of HCl 6 M (*ca.* 4 mL) and a precipitate was formed. The solution was centrifugated and AcOEt was added to the supernatant. The organic phase was washed with water. The organic layer was dried over Na_2SO_4 and the solvent was removed under reduced pressure. The product was purified by HPLC to give a white powder (88 mg, 48 % calculated based of the formula **L-Ar-NHAc(*t*Bu)$_3$·3TFA**). HPLC (anal.): t_R = 9.4 min (method B); ^{1}H NMR (400 MHz, CD_3OD): δ = 8.41 (s, 1H), 8.01 (d, J = 1.5, 1H), 7.76 (s, 4H), 4.67 (s, 2H), 4.20-3.10 (m, 22H), 2.17 (s, 3H), 1.48 (s, 9H), 1.32 (s, 18H); $^{13}C\{^1H\}$ NMR (100 MHz, CD_3OD): δ = 171.9, 167.4, 162.5 (q, J = 38, TFA), 151.6, 149.8, 142.1, 132.7, 128.8, 126.1, 123.3, 121.4, 118.0 (q, J = 291, TFA), 85.4, 84.2, 58.4, 56.0, 55.2, 52.6, 50.7, 28.4, 24.0; HRMS (ESI+): monoisotopic *m/z* = 783.4655 (+) / calculated *m/z* = 783.4651 $[M+H]^+$ for M = $C_{41}H_{62}N_6O_9$.

***tert*-butyl(3-((4-iodo-3-methylphenyl)amino)-3-oxopropyl)carbamate (5a):** 4-iodo-3-methylaniline (595 mg, 2.6 mmol) was dissolved in DCM (5 mL) with Boc-β-Ala-OH (478 mg, 2.5 mmol) and DMAP (16.5 mg, 0.2 mmol). The solution was stirred for 10 min at 0 °C; then DCC (524 mg, 2.5 mmol) was added and a precipitate was formed. The solution was stirred at 0 °C to room temperature for 4 h. The reaction mixture was diluted in DCM and filtered. The organic phase was washed using a saturated $NaHCO_3$ then water. The organic layer was dried over Na_2SO_4 and the solvent was removed under reduced pressure. The crude product was purified by flash chromatography (silica gel, AcOEt/cyclohexane 20:80) to give a colourless powder (810 mg, 79 %). ^{1}H NMR (400 MHz, $CDCl_3$): δ = 7.82 (br, 1H), 7.70 (d, J = 8.5, 1H), 7.49 (s, 1H), 7.09 (d, J = 8.5, 1H), 5.13 (b, 1H), 3.48 (m), 2.58 (t, J = 11.5, 2H), 2.39 (s, 3H), 1.43 (s, 9H); $^{13}C\{^1H\}$ NMR (100 MHz, $CDCl_3$): δ = 169.7, 142.1, 139.2, 138.2, 121.0, 118.9, 94.4, 79.8, 37.8, 36.4, 28.4, 28.2; LRMS (ESI+): monoisotopic *m/z* = 405.0 (+), 427.0 (+) / calculated *m/z* = 405.0 $[M+H]^+$, 427.0 $[M+Na]^+$ for M = $C_{15}H_{21}N_2O_3I$.

***tert*-butyl(3-((3-methyl-4-(4,4,5,5-tetramethyl-1,3,2-dioxaborolan-2-yl)phenyl)amino)-3-oxopropyl)carbamate (5)**: Compound **5a** (463 mg, 1.1 mmol), *bis*(pinacolato)diboron (305 mg, 1.2 mmol), [1,1'-*bis*(diphenylphosphino)-ferrocene]palladium(II) dichloride (40 mg, 0.05 mmol) and sodium acetate (215 mg, 2.6 mmol) were dissolved in dried DMSO (2 mL). The solution was degassed using argon during 45 min. The reaction was stirred at 90 °C under argon for 18 h then cooled to room temperature. The reaction mixture was diluted in AcOEt and filtrated over Celite. The organic layer was washed with saturated NH_4Cl twice and then with water. The organic layer was dried over Na_2SO_4 and the solvent was removed under reduced pressure. The crude product was purified by flash chromatography (silica gel, AcOEt/cyclohexane 10:90) to give a slightly yellow oil (263 mg, 59 %). ^{1}H NMR (400 MHz, $CDCl_3$): δ = 7.74 (d, J = 8.0, 1H), 7.59 (br, 1H), 7.39 (s, 1H), 7.34 (d, J = 8.0, 1H), 5.19 (b, 1H), 3.51 (m, 2H), 2.62 (t, J = 11.5, 2H), 2.54 (s, 3H), 1.46 (s, 9H), 1.36 (s, 12H); ^{13}C{^{1}H} NMR (100 MHz, $CDCl_3$): δ = 182.0, 167.7, 146.4, 139.9, 137.1, 120.4, 115.6, 83.4, 37.7, 36.5, 28.4, 28.4, 24.9, 22.3; LRMS (ESI+): monoisotopic m/z = 405.0 (+) / calculated m/z = 405.3 $[M+H]^+$ for M = $C_{21}H_{33}N_2O_5B$.

L-^{Me}Ar-NH(BocβAla)(*t*Bu)$_3$: Compound **5** (187 mg, 0.44 mmol), compound **1** (300 mg, 0.38 mmol), cesium fluoride (173 mg, 1.14 mmol) and *tetrakis*(triphenylphosphine)palladium(0) (95 mg, 0.038 mmol) were dissolved in anhydrous DMF (3 mL). The reaction was stirred at 90 °C under argon for 20 h then cooled to room temperature. The reaction mixture was diluted using AcOEt and filtrated over Celite. The solution was extracted with saturated $NaHCO_3$ then water. The organic layer was dried over Na_2SO_4 and the solvent was removed under reduced pressure. The crude product was dissolved in EtOH (20 mL). NaOH 6 M (4 mL) was added dropwise and the reaction mixture was stirred for 10 min at room temperature. The solution was neutralized by dropwise addition of HCl 6 M (*ca.* 4 mL) and a precipitate was formed. The suspension was centrifugated and the supernatant was removed under reduced and the residue was solubilized in AcOEt. The solution was washed with water, dried over Na_2SO_4 and the solvent was removed under reduced pressure. The product obtained was purified by HPLC to give a white powder (259 mg, 49 % calculated based of the formula **L-Ar-NH(BocβAla)(*t*Bu)$_3$·4TFA**). HPLC (anal.): t_R = 10.7 min (method B); ^{1}H NMR (400 MHz, CD_3OD): δ = 8.17 (s, 1H), 7.74 (d, J = 1.0, 1H), 7.62 (s, 1H), 7.60 (s, 1H), 7.26 (d, J = 8.5, 1H), 4.69 (s, 2H), 4.27-3.47 (br, 18H), 3.43 (t, J = 7.0, 2H), 3.31-2.92 (br, 6H), 2.60 (t, J = 7.0, 2H), 2.36 (s, 3H), 1.51 (s, 9H), 1.45 (s, 9H), 1.36 (s, 18H); ^{13}C{^{1}H} NMR (100 MHz, CD_3OD): δ = 172.5, 167.4, 162.2 (q, J = 38, TFA), 153.2, 149.0, 140.9, 137.1, 134.2, 131.2, 129.4, 126.8, 123.2, 117.7 (q, J = 291, TFA), 116.3, 84.0, 80.2, 58.1, 56.0, 55.1, 52.5, 50.6, 38.3, 37.9, 28.7, 28.4, 20.8; LRMS (ESI+): monoisotopic m/z = 926.5 (+) / calculated m/z = 926.6 $[M+H]^+$, for M = $C_{48}H_{75}N_7O_{11}$; HRMS (ESI+): monoisotopic m/z = 926.5581 (+) / calculated m/z = 926.5597 $[M+H]^+$ for M = $C_{48}H_{75}N_7O_{11}$.

***tert*-butyl 4-((4-iodo-3-methylphenyl)amino)-4-oxobutanoate (6a) :** 4-iodo-3-methylaniline (595 mg, 2.6 mmol) was dissolved in DCM (5 mL) with 4-(tert-butoxy)-4-oxobutanoic acid (436 mg, 2.5 mmol) and DMAP (16.5 mg, 0.2 mmol). The solution was stirred for 10 min at 0 °C; then DCC (524 mg, 2.5 mmol) was added and a precipitate was formed. The solution was stirred at 0 °C to room temperature for 4 h. The reaction mixture was diluted in DCM and filtered. The organic phase was washed using a saturated $NaHCO_3$ then water. The organic layer was dried over Na_2SO_4 and the solvent was removed under reduced pressure. The crude product was purified by flash chromatography (silica gel, AcOEt/cyclohexane 30:70) to give a colourless oil (732 mg, 75 %). ^{1}H NMR (400 MHz, $CDCl_3$): δ = 7.89 (br, 1H), 7.69 (d, J = 8.5, 1H), 7.47 (s, 1H), 7.07 (d, J = 8.5, 1H), 2.72-2.57 (m, 4H), 2.40 (s, 3H), 1.48 (s, 9H); ^{13}C{^{1}H} NMR (100 MHz, $CDCl_3$): δ = 172.7, 170.1, 142.0, 139.1, 138.2, 120.9, 118.8, 94.1, 81.4, 34.0, 32.5, 30.8, 28.1; LRMS (ESI+): monoisotopic m/z = 390.0 (+), 412.0 (+) / calculated m/z = 390.0 $[M+H]^+$, 412.0 $[M+Na]^+$ for M = $C_{15}H_{20}NO_3I$.

***tert*-butyl 4-((3-methyl-4-(4,4,5,5-tetramethyl-1,3,2-dioxaborolan-2-yl)phenyl)amino)-4-oxobutanoate (6)**: Compound **6a** (446 mg, 1.1 mmol), *bis*(pinacolato)diboron (307 mg, 1.2 mmol), [1,1'-*bis*(diphenylphosphino)-ferrocene]palladium(II) dichloride (41 mg, 0.05 mmol) and sodium acetate (237 mg, 2.9 mmol) were dissolved in dried

DMSO (2 mL). The solution was degassed using argon during 45 min. The reaction was stirred during 18 h at 90 °C under argon. The reaction mixture was diluted in AcOEt and filtrated over Celite. The organic layer was washed with saturated NH_4Cl twice and then with water. The organic layer was dried over Na_2SO_4 and the solvent was removed under reduced pressure. The crude product was purified by flash chromatography (silica gel, AcOEt/cyclohexane 20:80) to give a slightly yellow oil (269 mg, 60 %). ^{1}H NMR (400 MHz, $CDCl_3$): δ = 7.72 (d, J = 8.0, 1H), 7.36 (s, 1H), 7.32 (d, J = 8.0, 1H), 2.70-2.59 (m, 4H), 2.53 (s, 3H), 1.47 (s, 9H), 1.35 (s, 12H); ^{13}C{^{1}H} NMR (100 MHz, $CDCl_3$): δ = 172.6, 170.1, 146.3, 140.2, 137.0, 120.4, 115.6, 83.3, 81.2, 32.6, 30.9, 30.8, 28.1, 24.9, 22.3; LRMS (ESI+): monoisotopic *m/z* = 390.0 (+) / calculated *m/z* = 390.2 $[M+H]^+$, for M = $C_{21}H_{32}NO_5B$.

L-^{Me}Ar-NH(*t*BuSuc)(*t*Bu)$_3$: Compound **6** (185 mg, 0.48 mmol), compound **1** (300 mg, 0.38 mmol), cesium fluoride (173 mg, 1.14 mmol) and *tetrakis*(triphenylphosphine)palladium(0) (95 mg, 0.038 mmol) were dissolved in anhydrous DMF (3 mL). The reaction was stirred at 90 °C under argon for 20 h then cooled to room temperature. The reaction mixture was diluted using AcOEt and filtrated over Celite. The solution was extracted with saturated $NaHCO_3$ then water. The organic layer was dried over Na_2SO_4 and the solvent was removed under reduced pressure. The crude product was dissolved in EtOH (20 mL). NaOH 6 M (4 mL) was added dropwise and the reaction mixture was stirred for 10 min at room temperature. The solution was neutralized by dropwise addition of HCl 6 M (*ca.* 4 mL) and a precipitate was formed. The suspension was centrifugated and the supernatant was removed under reduced and the residue was solubilized in AcOEt. The solution was washed with water, dried over Na_2SO_4 and the solvent was removed under reduced pressure. The product obtained was purified by HPLC to give a white powder (266 mg, 56 % calculated based of the formula **L-^{Me}Ar-NH(*t*BuSuc)(*t*Bu)$_3$·3TFA**). HPLC (anal.): t_R = 9.3 min (method B); ^{1}H NMR (400 MHz, CD_3OD): δ = 8.17 (s, 1H), 7.75 (d, J = 1.0, 1H), 7.61 (s, 1H), 7.59 (s, 1H), 7.26 (d, J = 8.5, 1H), 4.70 (s, 2H), 4.39-2.89 (br, 22H), 2.67 (m, 4H), 2.36 (s, 3H), 1.51 (s, 9H), 1.47 (s, 9H), 1.35 (s, 18H); ^{13}C{^{1}H} NMR (100 MHz, CD_3OD): δ = 173.6, 173.0, 162.2 (q, J = 38, TFA), 153.2, 149.0, 142.9, 141.0, 137.1, 134.1, 131.2, 129.5, 126.7, 123.0, 119.0 (q, J = 291, TFA), 116.3, 84.0, 81.8, 58.1, 56.0, 55.1, 52.5, 50.6, 32.5, 31.4, 28.4, 28.3, 20.8; LRMS (ESI+): monoisotopic *m/z* = 911.5 (+) / calculated *m/z* = 911.5 $[M+H]^+$, for M = $C_{48}H_{74}N_6O_{11}$; HRMS (ESI+): monoisotopic *m/z* = 911.5464 (+) / calculated *m/z* = 911.5488 $[M+H]^+$ for M = $C_{48}H_{74}N_6O_{11}$.

Peptide sequences

AcK-TAT-RA resin: Ac-Lys-Arg(Pbf)-Lys(Boc)-Lys(Boc)-Arg(Pbf)-Arg(Pbf)-Gln(Trt)-Arg(Pbf)-Arg(Pbf)-Arg(Pbf)-Gly-Rink Amide resin
CK-TAT-RA resin: Boc-Cys(Trt)-Lys-Arg(Pbf)-Lys(Boc)-Lys(Boc)-Arg(Pbf)-Arg(Pbf)-Gln(Trt)-Arg(Pbf)-Arg(Pbf)-Arg(Pbf)-Gly-Rink Amide resin

mTAT[L-^{Me}Ar-OMe]: Ac-K(L-^{Me}Ar-OMe)RKKRRQRRRG-NH_2
mTAT[Eu·L-^{Me}Ar-OMe]: Ac-K(Eu·L-^{Me}Ar-OMe)RKKRRQRRRG-NH_2
mTAT[Tb·L-^{Me}Ar-OMe]: Ac-K(Tb·L-^{Me}Ar-OMe)RKKRRQRRRG-NH_2
mTAT[Gd·L-^{Me}Ar-OMe]: Ac-K(Gd·L-^{Me}Ar-OMe)RKKRRQRRRG-NH_2
CTAT[L-^{Me}Ar-OMe]: CK(L-^{Me}Ar-OMe)RKKRRQRRRG-NH_2
dTAT[Tb·L-^{Me}Ar-OMe]: (CK(Tb·L-^{Me}Ar-OMe)RKKRRQRRRG-$NH_2)_2$ (disulfide bridge)

mTAT[L-^{Me}Ar-NHAc]: Ac-K(L-^{Me}Ar-NHAc)RKKRRQRRRG-NH_2
mTAT[Eu·L-^{Me}Ar-NHAc]: Ac-K(Eu·L-^{Me}Ar-NHAc)RKKRRQRRRG-NH_2
mTAT[Tb·L-^{Me}Ar-NHAc]: Ac-K(Tb·L-^{Me}Ar-NHAc)RKKRRQRRRG-NH_2
mTAT[Gd·L-^{Me}Ar-NHAc]: Ac-K(Gd·L-^{Me}Ar-NHAc)RKKRRQRRRG-NH_2
CTAT[L-^{Me}Ar-NHAc]: CK(L-^{Me}Ar-NHAc)RKKRRQRRRG-NH_2
dTAT[Tb·L-^{Me}Ar-NHAc]: (CK(Tb·L-^{Me}Ar-NHAc)RKKRRQRRRG-$NH_2)_2$ (disulfide bridge)

mTAT[L-Ar-NHAc]: Ac-K(L-^{Me}Ar-NHAc)RKKRRQRRRG-NH_2
mTAT[Eu·L-Ar-NHAc]: Ac-K(Eu·L-^{Me}Ar-NHAc)RKKRRQRRRG-NH_2
mTAT[Tb·L-Ar-NHAc]: Ac-K(Tb·L-^{Me}Ar-NHAc)RKKRRQRRRG-NH_2
mTAT[Gd·L-Ar-NHAc]: Ac-K(Gd·L-^{Me}Ar-NHAc)RKKRRQRRRG-NH_2
CTAT[L-Ar-NHAc]: CK(L-^{Me}Ar-NHAc)RKKRRQRRRG-NH_2
dTAT[Tb·L-Ar-NHAc]: (CK(Tb·L-^{Me}Ar-NHAc)RKKRRQRRRG-$NH_2)_2$ (disulfide bridge)

CTAT[L-^{Me}Ar-NHβAla(+)]: CK(L-^{Me}Ar-NHβAla(+))RKKRRQRRRG-NH_2
dTAT[Tb·L-^{Me}Ar-NHβAla(+)]: (CK(Tb·L-^{Me}Ar-NHβAla(+))RKKRRQRRRG-$NH_2)_2$ (disulfide bridge)

CTAT[L-^{Me}Ar-NHSuc(–)]: CK(L-^{Me}Ar-NHSuc(–))RKKRRQRRRG-NH_2
dTAT[Tb·L-^{Me}Ar-NHSuc(–)]: (CK(Tb·L-^{Me}Ar-NHSuc(–))RKKRRQRRRG-$NH_2)_2$ (disulfide bridge)

Peptide synthesis

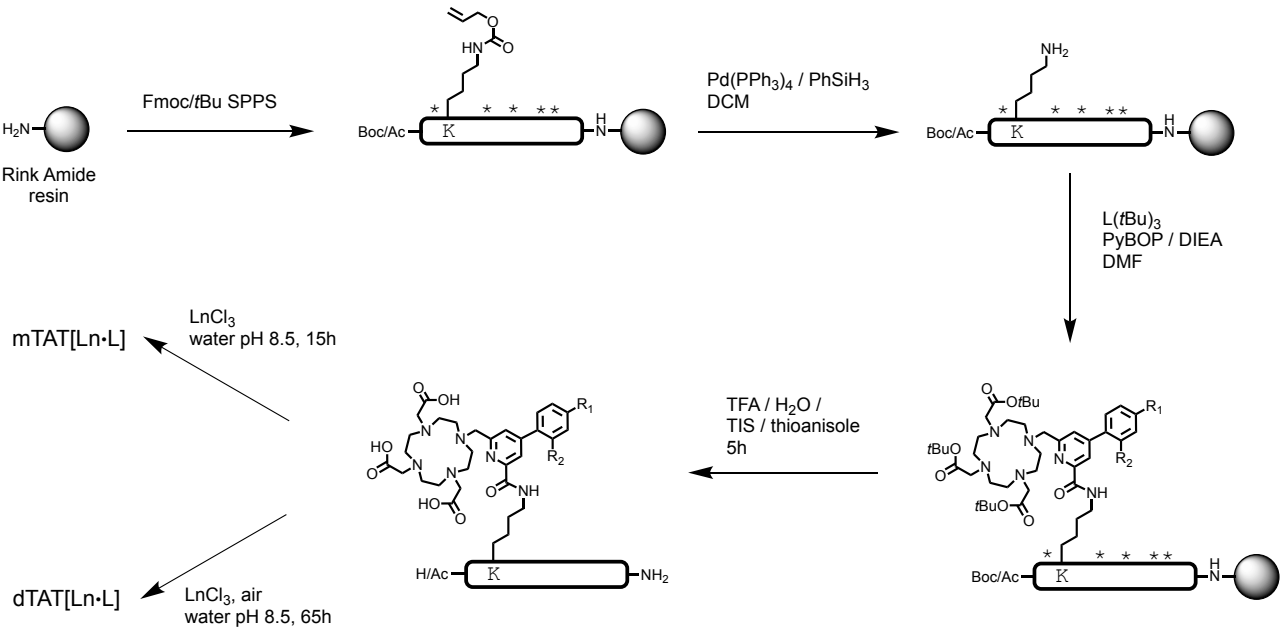

Fig. S2 Synthetic pathways for conjugates **mTAT[Ln·L]** and **dTAT[Ln·L]**. * denotes side chain protecting standard groups for Fmoc/tBu SPPS.

Peptide elongation: Peptide elongation was performed using standard SPPS procedure using Fmoc/*t*Bu chemistry on an automated peptide synthesizer (CEM Liberty1 Microwave Peptide Synthesizer) under microwave irradiation following protocols established by CEM[6] with double coupling. Fmoc removal was performed using 20 % piperidine in DMF. Couplings were performed using 4-fold molar excess of Fmoc-L-amino acid (0.2 M in DMF), 3.6-fold molar excess of HCTU (0.45 M in DMF) and 8-fold molar excess of DIEA (2 M in NMP).

AcK-TAT-RA resin: The peptide was synthesized on Rink-PEG-PS resin (NovaPEG Rink Amide, 0.25 mmol, 0.4 mmol/g). Automated peptide elongation was performed as described above using Fmoc-Lys(Alloc)-OH to introduce the N-terminal lysine. After the final Fmoc removal, the N-terminus was acetylated using Ac_2O/pyridine/DMF (1:2:7 v/v/v, 10 mL, 5 min). Removal of the Alloc protecting group was performed by adding a solution of *tetrakis*(triphenylphosphine)palladium(0) (0.073 mmol, 0.34 eq., 85 mg) and phenylsilane (12.5 mmol, 50 eq., 1.5 mL) in DCM (10 mL) for 1 h in the dark (twice).[7] The resin was then washed successively with DCM (2×2 min), DMF (2×2 min), 1 % H_2O in DMF (2×2 min), DMF (2×2 min), 1 % DIEA in DMF (2×2 min), DMF (2×2 min), sodium diethyldithiocarbamate in DMF (0.12 M, 2×5 min), DMF (2×2 min). The resin was dried and stored at -20 °C.

CK-TAT-RA resin: The peptide was synthesized on Rink-PEG-PS resin (NovaPEG Rink Amide, 0.25 mmol, 0.4 mmol/g). Automated peptide elongation was performed as described above using Fmoc-Lys(Alloc)-OH to introduce the last lysine and Boc-Cys(Trt)-OH to introduce the N-terminal cysteine. Removal of the Alloc protecting group was performed as described above for **AcK-TAT-RA resin**.

General procedure for mTAT[L] and CTAT[L]: The synthesis was performed on the 10 µmol scale. **L(*t*Bu)$_3$** (15 µmol, 1.5 eq.) was coupled to the peptide with PyBOP (50 µmol, 5 eq.) and DIEA (50 µL, 30 eq) in DMF (2 mL). Removal of acid-labile side chain protecting groups and resin cleavage were performed using TFA/H_2O/TIS/thioanisole (91:3:3:3 v/v/v/v, 2 mL) for 4 h. The solvent was evaporated under reduced pressure and cold Et_2O was added to precipitate the peptide. The suspension was centrifuged, the solid was washed twice with Et_2O and purified by HPLC. After freeze-drying, the conjugate was obtained as a white powder (*ca.* 5-10 mg).

mTAT[L-^{Me}Ar-OMe]: HPLC (anal.): t_R = 6.4 min (method B); LRMS (ESI+): average *m/z* = 1076.2 (2+), 717.5 (3+),

538.7 (4+), 431.2 (5+), 359.5 (6+) / calculated av. *m/z* = 1075.78 $[M+2H]^{2+}$, 717.51 $[M+3H]^{3+}$, 538.39 $[M+4H]^{4+}$, 430.91 $[M+5H]^{5+}$, 359.26 $[M+6H]^{6+}$ for M = $C_{92}H_{161}N_{39}O_{21}$); deconvoluted mass found = 2150.4 / expected mass = 2149.52 (average isotopic composition).

CTAT[L-^{Me}Ar-OMe]: HPLC (anal.): t_R = 6.3 min (method B); LRMS (ESI+): average *m/z* = 1106.3 (2+), 738.0 (3+), 553.9 (4+), 444.3 (5+), 369.7 (6+) / calculated av. *m/z* = 1106.32 $[M+2H]^{2+}$, 737.88 $[M+3H]^{3+}$, 553.66 $[M+4H]^{4+}$, 443.13 $[M+5H]^{5+}$, 369.44 $[M+6H]^{6+}$ for M = $C_{93}H_{164}N_{40}O_{21}S$); deconvoluted mass found = 2211.6 / expected mass = 2210.62 (average isotopic composition).

mTAT[L-^{Me}Ar-NHAc]: HPLC (anal.): t_R = 5.8 min (method B); LRMS (ESI+): average *m/z* = 726.6 (3+), 545.3 (4+), 436.5 (5+), 363.9 (6+), 312.1 (7+) / calculated av. *m/z* = 726.52 $[M+3H]^{3+}$, 545.14 $[M+4H]^{4+}$, 436.32 $[M+5H]^{5+}$, 363.76 $[M+6H]^{6+}$, 311.94 $[M+7H]^{7+}$ for M = $C_{93}H_{162}N_{40}O_{21}$); deconvoluted mass found = 2277.2 / expected mass = 2176.54 (average isotopic composition).

CTAT[L-^{Me}Ar-NHAc]: HPLC (anal.): t_R = 5.8 min (method B); LRMS (ESI+): average *m/z* = 746.9 (3+), 560.6 (4+), 448.8 (5+), 374.1 (6+) / calculated av. *m/z* = 746.89 $[M+3H]^{3+}$, 560.42 $[M+4H]^{4+}$, 448.54 $[M+5H]^{5+}$, 373.95 $[M+6H]^{6+}$ for M = $C_{94}H_{165}N_{41}O_{21}S$); deconvoluted mass found = 2238.9 / expected mass = 2237.65 (average isotopic composition).

mTAT[L-Ar-NHAc]: HPLC (anal.): t_R = 5.7 min (method B); LRMS (ESI+): average *m/z* = 722.0 (3+), 541.8 (4+), 433.8 (5+), 361.7 (6+) / calculated av. *m/z* = 721.85 $[M+3H]^{3+}$, 541.64 $[M+4H]^{4+}$, 433.51 $[M+5H]^{5+}$, 361.43 $[M+6H]^{6+}$ for M = $C_{92}H_{160}N_{40}O_{21}$); deconvoluted mass found = 2163.6 / expected mass = 2162.52 (average isotopic composition).

CTAT[L-Ar-NHAc]: HPLC (anal.): t_R = 5.6 min (method B); LRMS (ESI+): average *m/z* = 742.0 (3+), 556.8 (4+), 445.7 (5+) / calculated av. *m/z* = 742.22 $[M+3H]^{3+}$, 556.91 $[M+4H]^{4+}$, 445.73 $[M+5H]^{5+}$, 371.61 $[M+6H]^{6+}$ for M = $C_{93}H_{163}N_{41}O_{21}S$); deconvoluted mass found = 2223.2 / expected mass = 2223.62 (average isotopic composition).

CTAT[L-^{Me}Ar-NHβAla(+)]: HPLC (anal.): t_R = 5.3 min (method B); LRMS (ESI+): average *m/z* = 756.5 (4+), 567.8 (4+), 454.4 (5+), 378.9 (6+), 324.9 (7+) / calculated av. *m/z* = 756.57 $[M+3H]^{3+}$, 567.67 $[M+4H]^{4+}$, 454.34 $[M+5H]^{5+}$, 378.79 $[M+6H]^{6+}$, 324.82 $[M+7H]^{7+}$ for M = $C_{95}H_{168}N_{42}O_{21}S$); deconvoluted mass found = 2266.9 / expected mass = 2266.68 (average isotopic composition).

CTAT[L-^{Me}Ar-NHSuc(–)]: HPLC (anal.): t_R = 5.6 min (method B); LRMS (ESI+): average *m/z* = 766.2 (3+), 575.0 (4+), 460.3 (5+), 383.8 (6+) / calculated av. *m/z* = 766.23 $[M+3H]^{3+}$, 574.93 $[M+4H]^{4+}$, 460.14 $[M+5H]^{5+}$, 383.62 $[M+6H]^{6+}$ for M = $C_{96}H_{167}N_{41}O_{23}S$); deconvoluted mass found = 2296.7 / expected mass = 2295.68 (average isotopic composition).

General procedure for mTAT[LnL] complexes: Compound **mTAT[L]** (*ca.* 3 mg) and $LnCl_3{\cdot}(H_2O)_6$ (10 eq.) were dissolved in H_2O (0.6 mL) and the pH was adjusted to 7.5 using NaOH. The solution was stirred overnight at room temperature. The pH was decreased to *ca.* 3 using HCl before HPLC purification. After freeze-drying, **mTAT[LnL]** was obtained as a white powder (90 %).

mTAT[Eu·L-^{Me}Ar-OMe]: HPLC (anal.): t_R = 6.4 min (method B); LRMS (ESI+): average *m/z* = 767.6 (3+), 575.9 (4+), 460.9 (5+), 384.3 (6+) / calculated av. *m/z* = 767.16 $[M+3H]^{3+}$, 575.62 $[M+4H]^{4+}$, 460.70 $[M+5H]^{5+}$, 384.08 $[M+6H]^{6+}$ for M = $C_{92}H_{158}N_{39}O_{21}Eu$); deconvoluted mass found = 2299.2 / expected mass = 2298.45 (average isotopic composition).

mTAT[Tb·L-^{Me}Ar-OMe]: HPLC (anal.): t_R = 6.3 min (method B); LRMS (ESI+): average *m/z* = 769.7 (3+), 577.8 (4+), 462.3 (5+), 385.5 (6+) / calculated av. *m/z* = 769.48 $[M+3H]^{3+}$, 577.36 $[M+4H]^{4+}$, 462.09 $[M+5H]^{5+}$, 385.24 $[M+6H]^{6+}$ for M = $C_{92}H_{158}N_{39}O_{21}Tb$); deconvoluted mass found = 2306.7 / expected mass = 2305.42 (average isotopic composition).

mTAT[Gd·Eu·L-^{Me}Ar-OMe]: HPLC (anal.): t_R = 6.3 min (method B); LRMS (ESI+): average *m/z* = 769.0 (3+), 577.2 (4+), 462.0 (5+), 385.3 (6+) / calculated av. *m/z* = 768.92 $[M+3H]^{3+}$, 576.95 $[M+4H]^{4+}$, 461.76 $[M+5H]^{5+}$, 384.96 $[M+6H]^{6+}$ for M = $C_{92}H_{158}N_{39}O_{21}Gd$); deconvoluted mass found = 2305.1 / expected mass = 2303.74 (average isotopic composition).

mTAT[Eu·L-^{Me}Ar-NHAc]: HPLC (anal.): t_R = 5.8 min (method B); LRMS (ESI+): average *m/z* = 776.5 (3+), 582.6 (4+), 466.3 (5+), 388.8 (6+) / calculated av. *m/z* = 776.17 $[M+3H]^{3+}$, 582.38 $[M+4H]^{4+}$, 466.10 $[M+5H]^{5+}$, 388.59 $[M+6H]^{6+}$ for M = $C_{93}H_{159}N_{40}O_{21}Eu$); deconvoluted mass found = 2327.1 / expected mass = 2325.48 (average isotopic

composition).

mTAT[Tb·L-^{Me}Ar-NHAc]: HPLC (anal.): t_R = 5.8 min (method B); LRMS (ESI+): average *m/z* = 778.6 (3+), 584.3 (4+), 467.7 (5+), 388.9 (6+) / calculated av. *m/z* = 778.49 $[M+3H]^{3+}$, 584.12 $[M+4H]^{4+}$, 467.50 $[M+5H]^{5+}$, 389.75 $[M+6H]^{6+}$ for M = $C_{93}H_{159}N_{40}O_{21}Tb$); deconvoluted mass found = 2333.3 / expected mass = 2332.44 (average isotopic composition).

mTAT[Gd·L-^{Me}Ar-NHAc]: HPLC (anal.): t_R = 5.7 min (method B); LRMS (ESI+): average *m/z* = 777.9 (3+), 583.8 (4+), 467.3 (5+), 389.7 (6+) / calculated av. *m/z* = 777.93 $[M+3H]^{3+}$, 583.70 $[M+4H]^{4+}$, 467.16 $[M+5H]^{5+}$, 389.47 $[M+6H]^{6+}$ for M = $C_{93}H_{159}N_{40}O_{21}Gd$); deconvoluted mass found = 2321.2 / expected mass = 2330.77 (average isotopic composition).

mTAT[Eu·L-Ar-NHAc]: HPLC (anal.): t_R = 5.6 min (method B); LRMS (ESI+): average *m/z* = 771.8 (3+), 579.0 (4+), 463.5 (5+), 386.4 (6+) / calculated av. *m/z* = 771.49 $[M+3H]^{3+}$, 578.87 $[M+4H]^{4+}$, 463.30 $[M+5H]^{5+}$, 386.25 $[M+6H]^{6+}$ for M = $C_{92}H_{157}N_{40}O_{21}Eu$); deconvoluted mass found = 2311.5 / expected mass = 2311.46 (average isotopic composition).

mTAT[Tb·L-Ar-NHAc]: HPLC (anal.): t_R = 5.7 min (method B); LRMS (ESI+): average *m/z* = 580.8 (4+), 464.8 (5+), 387.6 (6+) / calculated av. *m/z* = 580.61 $[M+4H]^{4+}$, 464.69 $[M+5H]^{5+}$, 387.41 $[M+6H]^{6+}$ for M = $C_{92}H_{157}N_{40}O_{21}Tb$); deconvoluted mass found = 2319.0 / expected mass = 2318.42 (average isotopic composition).

mTAT[Gd·L-Ar-NHAc]: HPLC (anal.): t_R = 5.6 min (method B); LRMS (ESI+): average *m/z* = 580.3 (4+), 464.4 (5+), 387.3 (6+) / calculated av. *m/z* = 580.19 $[M+4H]^{4+}$, 464.36 $[M+5H]^{5+}$, 387.13 $[M+6H]^{6+}$ for M = $C_{92}H_{157}N_{40}O_{21}Gd$); deconvoluted mass found = 2317.0 / expected mass = 2316.74 (average isotopic composition).

General procedure for dTAT[LnL] complexes: Compound **CTAT[L]** (*ca.* 3-5 mg) and $LnCl_3·(H_2O)_6$ (10 eq.) were dissolved in H_2O (0.6 mL) and the pH was adjusted to 8.5 using NaOH. The solution was stirred under air at room temperature and LCMS was used to monitor completeness of the metalation and of the formation of the disulfide bridge (slower). After 48-64 h on stirring, the pH was decreased to *ca.* 3 using HCl before HPLC purification. After freeze-drying, **dTAT[LnL]** was obtained as a white powder (90 %).

dTAT[Tb·L-^{Me}Ar-OMe]: HPLC (anal.): t_R = 6.6 min (method B); LRMS (ESI+): average *m/z* = 793.8 (6+), 677.2 (7+), 592.7 (8+), 526.9 (9+), 474.4 (10+), 431.3 (11+), 395.5 (12+) / calculated av. *m/z* = 947.21 [M+5H]5+, 789.51 $[M+6H]^{6+}$, 676.87 $[M+7H]^{7+}$, 592.39 $[M+8H]^{8+}$, 526.68 $[M+9H]^{9+}$, 474.11 $[M+10H]^{10+}$, 431.10 $[M+11H]^{11+}$, 395.26 $[M+12H]^{12+}$ for M = $C_{186}H_{320}N_{80}O_{42}S_2Tb_2$); deconvoluted mass found = 4733.4 / expected mass = 4731.04 (average isotopic composition).

dTAT[Tb·L-^{Me}Ar-NHAc]: HPLC (anal.): t_R = 6.1 min (method B); LRMS (ESI+): average *m/z* = 798.8 (6+), 684.8 (7+), 599.4 (8+), 532.8 (9+), 479.8 (10+), 436.3 (11+), 400.0 (12+) / calculated av. *m/z* = 798.52 $[M+6H]^{6+}$, 684.59 $[M+7H]^{7+}$, 599.14 $[M+8H]^{8+}$, 532.68 $[M+9H]^{9+}$, 479.52 $[M+10H]^{10+}$, 436.02 $[M+11H]^{11+}$, 399.76 $[M+12H]^{12+}$ for M = $C_{188}H_{322}N_{82}O_{42}S_2Tb_2$); deconvoluted mass found = 4786.6 / expected mass = 4786.09 (average isotopic composition).

dTAT[Eu·L-Ar-NHAc]: HPLC (anal.): t_R = 5.9 min (method B); LRMS (ESI+): average *m/z* = 949.8 (5+), 791.8 (6+), 678.8 (7+), 594.3 (8+), 528.3 (9+), 475.3 (10+), 432.3 (11+), 396.3 (12+) / calculated av. *m/z* = 949.63 $[M+5H]^{5+}$, 791.53 $[M+6H]^{6+}$, 678.59 $[M+7H]^{7+}$, 593.90 $[M+8H]^{8+}$, 528.02 $[M+9H]^{9+}$, 475.32 $[M+10H]^{10+}$, 432.20 $[M+11H]^{11+}$, 396.27 $[M+12H]^{12+}$ for M = $C_{186}H_{318}N_{82}O_{42}S_2Eu_2$); deconvoluted mass found = 4744.6 / expected mass = 4743.11 (average isotopic composition).

dTAT[Tb·L-^{Me}Ar-NHβAla(+)]: HPLC (anal.): t_R = 5.6 min (method B); LRMS (ESI+): average *m/z* = 693.0 (7+), 606.6 (8+), 539.3 (9+), 485.5 (10+), 441.5 (11+), 404.8 (12+) / calculated av. *m/z* = 692.48 $[M+7H]^{7+}$, 606.40 $[M+8H]^{8+}$, 539.14 $[M+9H]^{9+}$, 485.32 $[M+10H]^{10+}$, 441.29 $[M+11H]^{11+}$, 404.60 $[M+12H]^{12+}$ for M = $C_{190}H_{328}N_{84}O_{42}S_2Tb_2$); deconvoluted mass found = 4844.6 / expected mass = 4843.15 (average isotopic composition).

dTAT[Tb·L-^{Me}Ar-NHSuc(–)]: HPLC (anal.): t_R = 6.0 min (method B); LRMS (ESI+): average *m/z* = 818.0 (6+), 701.3 (7+), 613.9 (8+), 545.8 (9+), 491.3 (10+) / calculated av. *m/z* = 817.86 $[M+6H]^{6+}$, 701.17 $[M+7H]^{7+}$, 613.65 $[M+8H]^{8+}$, 545.58 $[M+9H]^{9+}$, 491.12 $[M+10H]^{10+}$ for M = $C_{192}H_{326}N_{82}O_{46}S_2Tb_2$); deconvoluted mass found = 4902.3 / expected mass = 4901.13 (average isotopic composition).

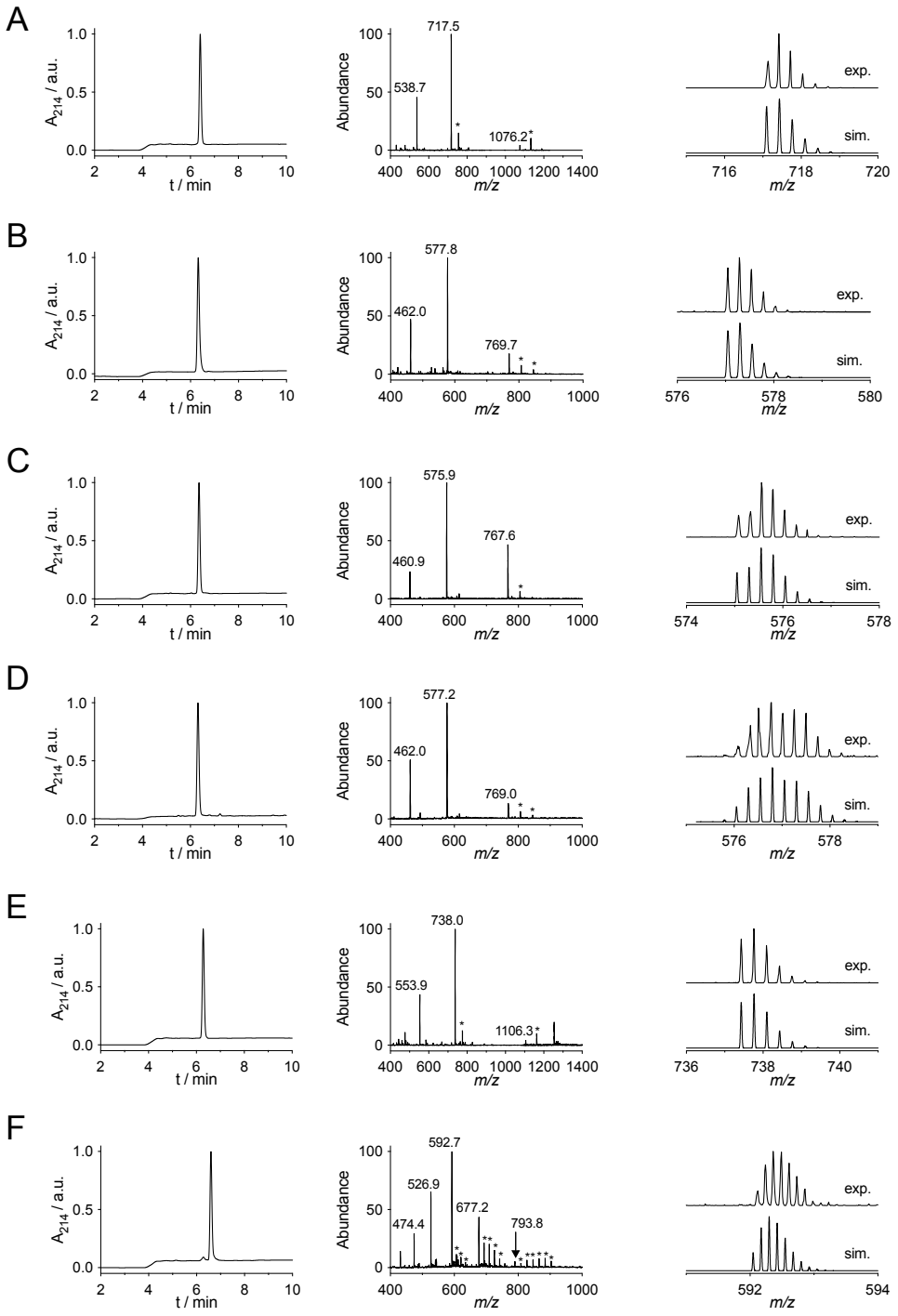

Fig. S3 Typical examples of HPLC chromatograms (*left*) and LRMS (ESI+) spectra (*middle*: full MS spectrum; *right*: experimental and simulated isotopic pattern) obtained for (A) **mTAT[L-^{Me}Ar-OMe]**, (B) **mTAT[Tb·L-^{Me}Ar-OMe]**, (C) **mTAT[Eu·L-^{Me}Ar-OMe]**, (D) **mTAT[Gd·L-^{Me}Ar-OMe]**, (E) **CTAT[L-^{Me}Ar-OMe]** and (F) **dTAT[Tb·L-^{Me}Ar-OMe]**. In full MS spectra, * indicates a TFA adduct.

1P spectroscopy

Determination of molar extinction coefficients: A solution of mTAT[L] or CTAT[L] peptide in HEPES buffer (10 mM, pH 7.5) was titrated by a solution of $TbCl_3$ or $EuCl_3$ of known concentration with absorption monitoring, as previously described.[8] The concentration of the peptide was determined from the endpoint of the titration, allowing determination of extinction coefficient using Beer Lambert law. The titration of mTAT[L-^{Me}Ar-OMe] by Tb^{3+} is given in Fig. S4 as typical example.

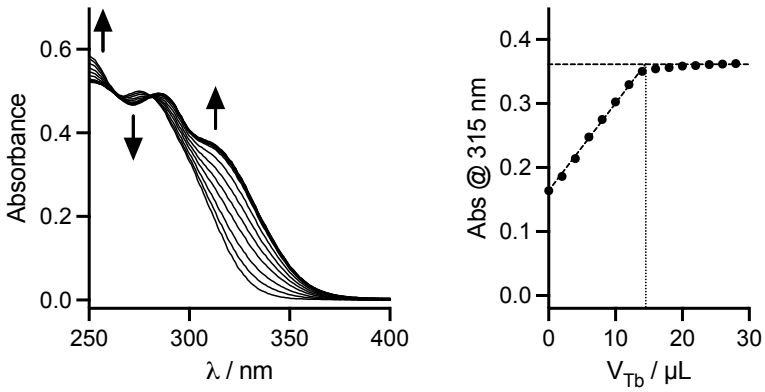

Fig. S4 Absorbance titration of mTAT[L-^{Me}Ar-OMe] in HEPES buffer (10 mM, pH 7.5, 1 mL) by $TbCl_3$ in H_2O (2.35 mM). Pathlength is 1.0 cm.

Absorption, excitation and emission spectra:

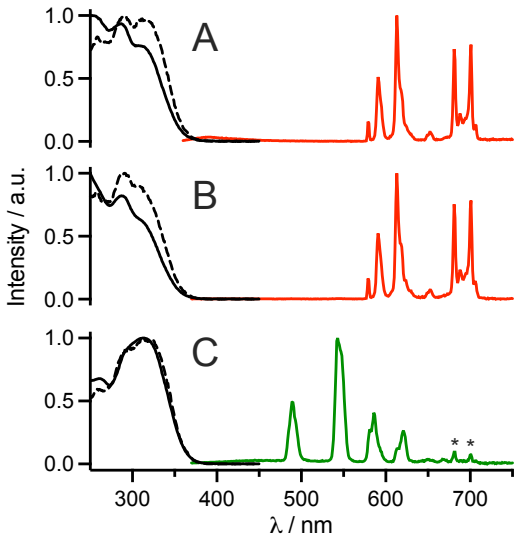

Fig. S5 Normalized absorption (black solid line), excitation (black dashed line; λ_{em} = 545 nm (A, B) or 615 nm (C)) and emission (colored solid line; λ_{ex} = 315 mn) spectra of (A) mTAT[Eu·L-^{Me}Ar-OMe], (B) mTAT[Eu·L-^{Me}Ar-NHAc] and (C) mTAT[Tb·L-Ar-NHAc] in PBS. In (C), * denotes Eu^{3+} contamination.

Luminescence decay: Ln^{3+} luminescence decays were measured for each compound in aerated and de-oxygenated PBS, prepared in H_2O, in aerated PBS prepared in D_2O and lifetimes, τ_{Ln}, were determined by mono-exponential fit (or bi-exponential fit when required). They are indicated in Table S1 as well as hydration number q determined using Parker's equations: $q^{Tb} = 5.0 \times (1/\tau(H_2O) - 1/\tau(D_2O) - 0.06)$ and $q^{Eu} = 1.2 \times (1/\tau(H_2O) - 1/\tau(D_2O) - 0.325))$ for Tb^{3+} and Eu^{3+},respectively, with τ in ms.[9] Examples of decay curves and their fits are given in Fig. S6.

Table S1: Luminescence lifetimes and hydration numbers q of mTAT[Ln·L] conjugates in PBS (λ_{ex} = 315 nm).[a]

Compound	Ln	τ_{Ln} / ms H_2O, aerated	τ_{Ln} / ms H_2O, de-oxygenated	τ_{Ln} / ms D_2O, aerated	q (± 0.2)
mTAT[Ln·L-^{Me}Ar-OMe]	Tb	2.11	2.38	2.41	0.0
	Eu	1.05	1.05	1.65	0.0
mTAT[Ln·L-^{Me}Ar-NHAc]	Tb	0.83	1.02	1.03	n.d.[b]
	Eu	1.05	1.05	1.65	0.0
mTAT[Ln·L-Ar-NHAc]	Tb	0.07	0.20	0.08	n.d.[b]
	Eu	1.05	1.05	1.63	0.0

[a] Error on τ and q values are estimated ± 0.03 ms and ± 0.2, respectively. [b] Since back energy transfer to the triplet state contributes significantly to Tb^{3+} $^5D_4$ state decay, estimation of q by Parker's equation is not reliable and thus, q was not calculated.

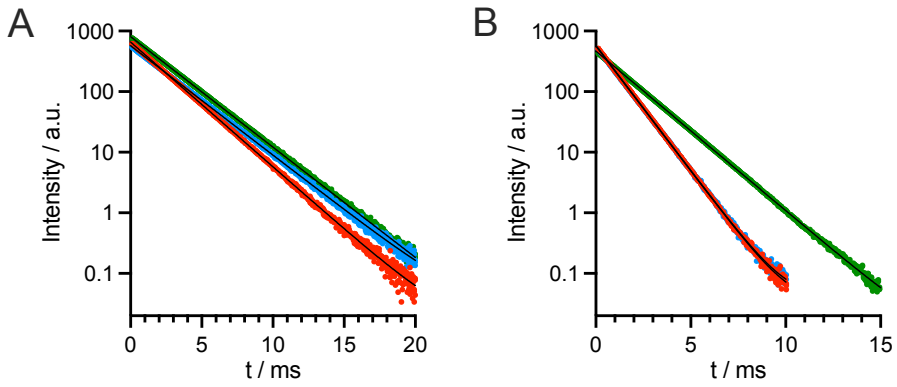

Fig. S6 Typical examples of luminescence decays and their mono-exponential fits measured for (A) mTAT[Tb·L-^{Me}Ar-OMe] and (B) mTAT[Eu·L-^{Me}Ar-OMe] in PBS (red: H_2O solution, aerated; blue: H_2O solution, de-oxygenated; green: D_2O solution, aerated). Lifetimes obtained by mono-exponential fits are given in Table S1.

Quantum yields measurements: Quantum yields were determined using a Fluorolog FL3-22 spectrophotometer by a relative method with quinine sulphate in 0.5 M H_2SO_4 as a reference compound (Φ = 0.545)[10,11] using solutions of various concentrations having absorption below 0.1 at the excitation wavelength. The excitation wavelength was the same for the sample compound (S) and the reference. To determine the quantum yields of the sample compound, the following equation was used:

$$\Phi_S = \frac{A_S}{I_S} \times \frac{I_{ref}}{A_{ref}} \times \frac{{n_S}^2}{{n_{ref}}^2} \times \Phi_{ref} \quad (1)$$

where A is the absorbance at the excitation wavelength, I the integrated emission intensity and n the refractive index. Estimated experimental error for the quantum yield determination is ~10 %. Fig. S7 shows data for mTAT[Ln·L-^{Me}Ar-OMe] as typical examples.

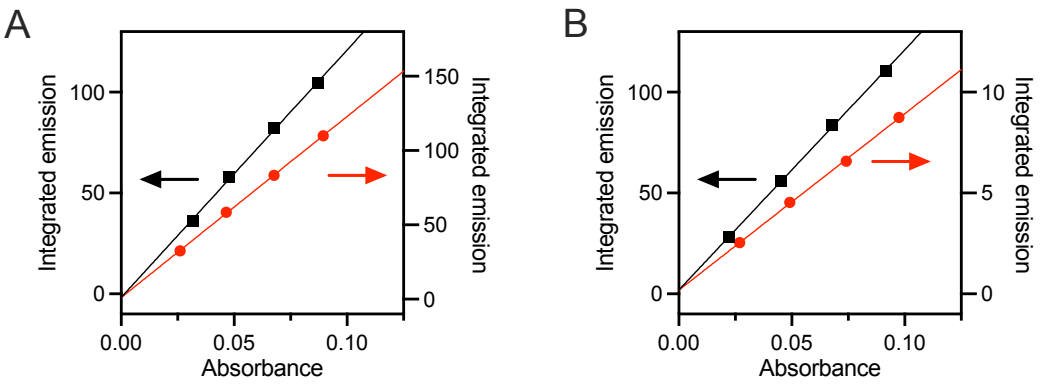

Fig. S7 Variation of integrated intensity against absorbance for (A) mTAT[Tb·L-^{Me}Ar-OMe] and (B) mTAT[Eu·L-^{Me}Ar-OMe] in PBS (red: conjugate; black: quinine sulfate). The slopes that correspond to *I*/*A* in Equation (1) were used to determine the quantum yields.

Determination of energy of S_1 and T_1 excited states: The energy of the S_1 state was determined using the cut-off of the absorption band. For the energy of T_1 excited state, a solution of the Gd-loaded peptide in PBS/glycerol 9:1 (v/v) was prepared and frozen at 77 K. A time-gated (delay = 100 µs) emission spectrum was recorded to monitor the antenna phosphorescence emission. The energy of the T_1 state was estimated using the wavelength at half-maximum on the onset of the phosphorescence spectrum.

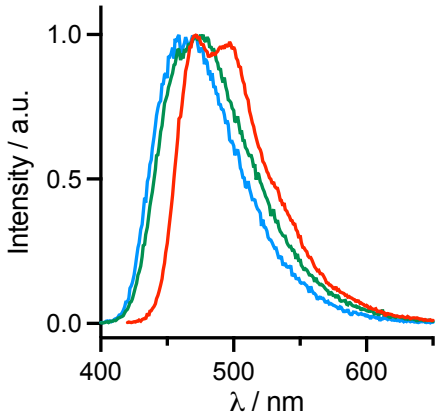

Fig. S8 Time-gated (100 µs delay) emission spectrum of mTAT[Gd·L-^{Me}Ar-OMe] (blue), mTAT[Gd·L-^{Me}Ar-NHAc] (green) and mTAT[Gd·L-Ar-NHAc] (red) in PBS/glycerol 9:1 (v/v) at 77 K (frozen solutions).

2P spectroscopy

Determination of 2P cross-sections σ_{2P}: Two-photon excitation spectra and two-photon cross-sections were obtained by two-photon excited fluorescence measurements of diluted PBS solutions of the compounds (*ca.* 10 µM, the exact concentration was determined from absorption spectrum) using a femtosecond Ti:sapphire laser (Coherent Chameleon Ultra II, 80 MHz, 140 fs) in the range 690–990 nm. The excitation beam (2.6 mm diameter) was focused with a 75 mm focal length lens to the sample. The up-converted fluorescence was collected at right-angle using a 30 mm focal length doublet lens. After filtering the scattered excitation beam by low-pass filters, the florescence was coupled to a fiber optic spectrometer (Avantes Hero). The sample was contained in a 1×1 cm quartz cell and continuously stirred with a magnetic stirrer to avoid thermal effects and photodegradation. After verifying that the emission intensity exhibited quadratic power

dependence for each sample (Fig. S9), the incident power was adjusted to 35 mW to characterize the two-photon absorption spectra. Calibration of the 2P absorption spectra was performed at each excitation wavelength by comparison with that of fluorescein (10 µM, pH 11) as reference compound.[12] 2P absorption spectra are provided in Fig. S10.

2P microscopy

General: HeLa, MRC5 and HEK293 cell lines were purchased from the ATCC and agreed by French ethic boards (CODECOH DC-2020-4226).

Cell culture: HeLa cells were grown in RPMI medium supplemented with 10% fetal bovine serum (v/v) at 37°C in a 5% CO_2 humidified atmosphere.

Peptides delivery in live cells: HeLa cells were seeded at 3×10^4 cells/well onto an 8-chamber Labtek-I coverglass system. After 24 h, cells were washed three times with PBS. Cells were incubated with dTAT [Ln·L] (10 µM) in RPMI medium (without phenol red and without serum) or PBS at 37°C for 1 h. Then, cells were washed three times with PBS before adding RPMI medium supplemented with fetal bovine serum (200 µL) for observation under microscope.

Confocal microscopy: Confocal 2P experiments were performed by using an LSM-DuoScan-Confocor3 NLO microscope (Carl Zeiss) composed of a LSM710 confocal module and an inverted motorized stand (AxioObserver) equipped with an on-stage cell incubator. Excitation was provided by a Ti:Sapphire femtosecond laser (Chameleon, Ultra II, Coherent) featuring chirp precompensation. The C-apochromat 40×/1.2 water-immersion objective was used throughout experiments. The pinhole was open during 2P acquisition in descanned detection mode. The spectral PMT detector (Quasar) or avalanche photodiodes were used to register the emission signal in each pixel of the confocal image. Temporal Sampling Lifetime Imaging Microscopy (TSLIM) was used to record luminescence lifetime decay in cells (single pulsed excitation with the 7.56 µs temporal resolution).[13]

Image analysis: Fiji/ImageJ was used to analyze images and particularly for linear unmixing to deconvolute autofluorescence and Ln^{3+} emission maps. They were performed using the Stowers ImageJ plugins developed by Jay Unruh at the Stowers Institute for Medical Research. Pure 2P-excited autofluorescence and Ln^{3+} emission spectra used for linear unmixing were acquired with the LSM710 microscope from control HeLa cells (Fig. S9) or droplets of mTAT[Ln·L] conjugates (100 µM in PBS). They are displayed in Fig. S10.

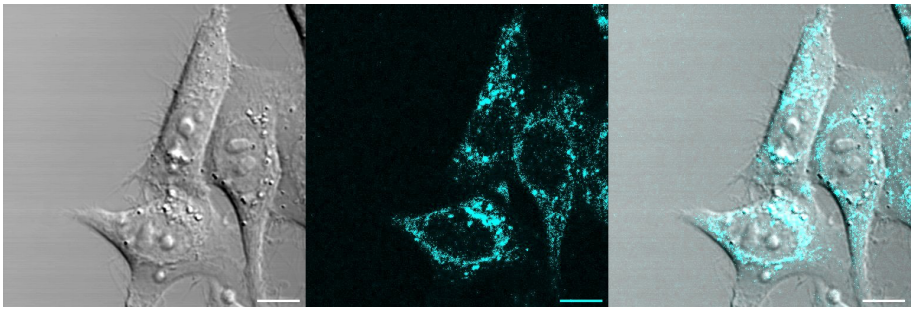

Fig. S9 2PM imaging (λ_{ex} = 720 nm) of control living HeLa cells (not incubated with dTAT[Ln·L]). Left panel shows the differential interference contrast (DIC) image, middle panel shows the luminescence image, and right panel shows the merge. Scale bar corresponds to 10 µm.

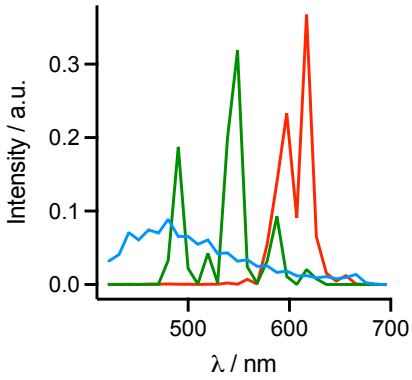

Fig. S10 2P-excited emission spectra of HeLa cell autofluorescence (blue), mTAT[Tb·L-^{Me}Ar-NHAc] (green) and mTAT[Eu·L-Ar-NHAc] (red) recorded with the LSM710 microscope (λ_{ex} = 720 nm).

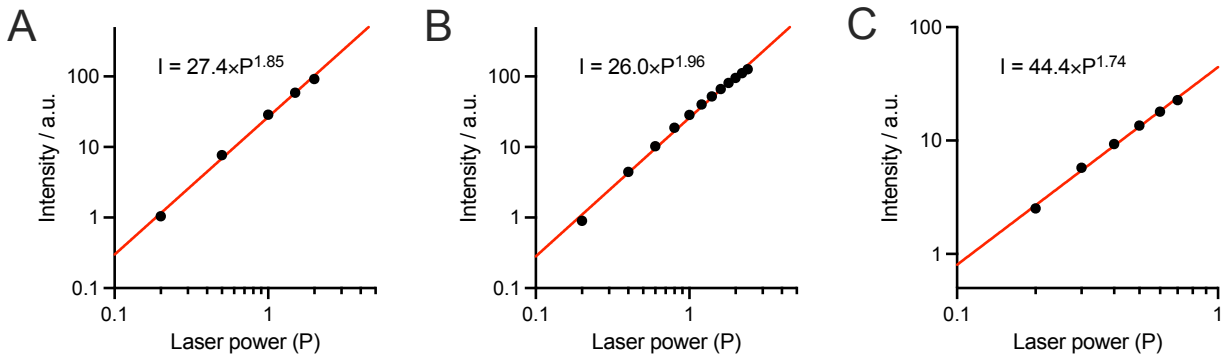

Fig. S11 Quadratic power dependence of the intensity of luminescence emission arising from HeLa cells incubated with (A) **dTAT[Tb·L-^{Me}Ar-OMe]**, (B) **dTAT[Tb·L-^{Me}Ar-NHAc]** and (C) **dTAT[Eu·L-Ar-NHAc]** (10 µM), detected with the LSM710 microscope PMT (λ_{ex} = 720 nm for A and C, 700 nm for B).

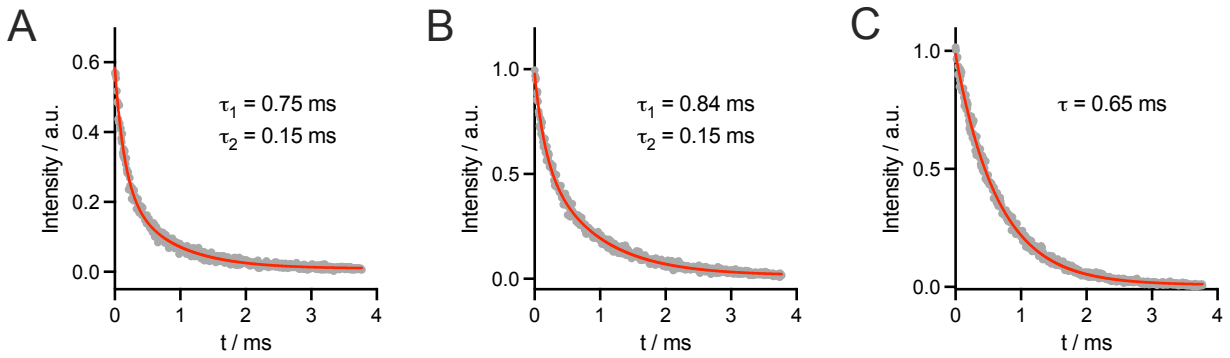

Fig. S12 Luminescence decay of (A) dTAT[Tb·L-^{Me}Ar-OMe], (B) dTAT[Tb·L-^{Me}Ar-NHAc] and (C) dTAT[Eu·L-Ar-NHAc] in HeLa cells (1 h incubation at 10 µM), recorded by TSLIM[13] with the LSM710 microscope (APD; λ_{ex} = 720 nm for A and C, 700 nm for B). Experimental data were fitted to bi-exponential (A and B) or mono-exponential (C) decays yielding τ values indicated on the graphs and in the text.

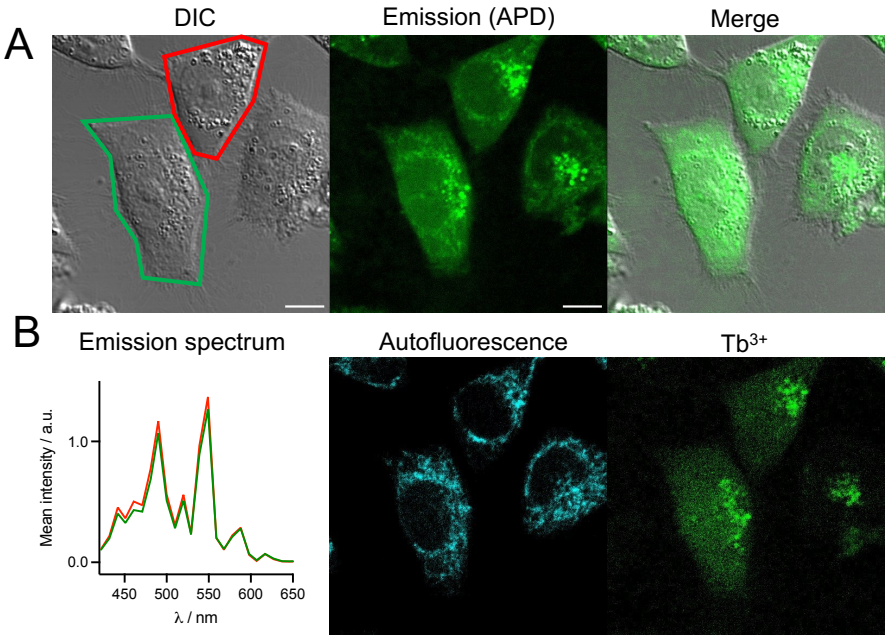

Fig. S13 2PM imaging (λ_{ex} = 720 nm) of living HeLa cells incubated 1 h with dTAT[Tb·L-^{Me}Ar-NHAc] (10 µM) in RPMI medium. (A) *Left panel:* DIC image; *Middle panel*: luminescence (detected with APD) image; *Right panel:* merge. Scale bars correspond to 10 µm. (B) *Left panel:* 2P-excited emission spectra (detection with PMT) of cells surrounded in red and green in panel A; *Middle and right panels:* autofluorescence and Tb^{3+} emission maps obtained by linear unmixing of 2P-excited spectral images recorded with the PMT.

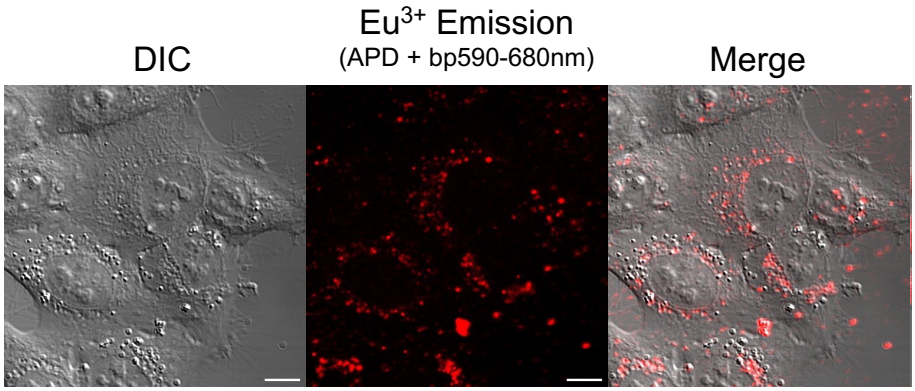

Fig. S14 2PM imaging (λ_{ex} = 720 nm) of living HeLa cells incubated 1 h with dTAT[Eu·L-Ar-NHAc] (2.5 µM) in RPMI medium. *Left panel:* DIC image; *Bottom left*: *Middle panel*: Eu^{3+} luminescence (detected with APD and a 590-680 nm band-pass filter) image; *Right panel:* merge. Scale bars correspond to 10 µm.

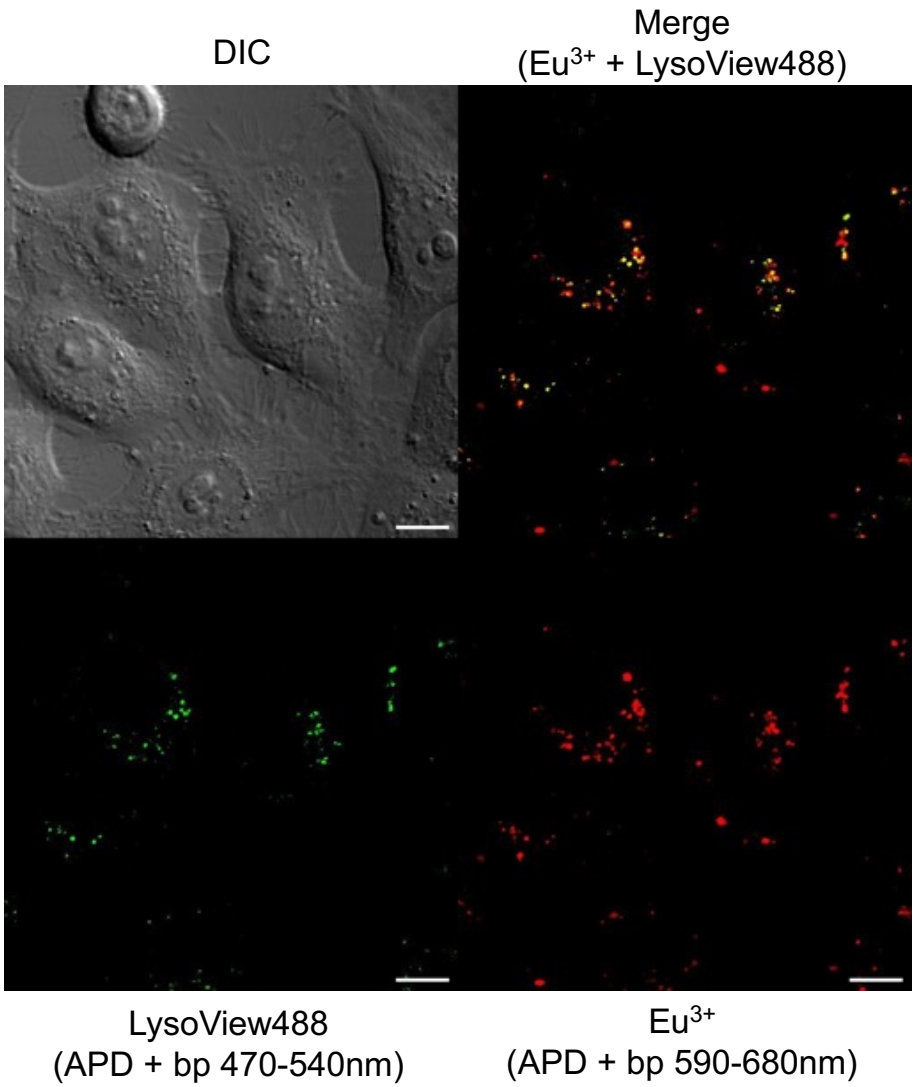

Fig. S15 2PM imaging (λ_{ex} = 720 nm) of living HeLa cells incubated 1 h with dTAT[Eu·L-Ar-NHAc] (2.5 µM) in RPMI medium and counter-stained with Lysoview488. *Top left panel:* DIC image; *Bottom left panel*: green channel / LysoView488 emission (detected with APD and a 470-540 nm band-pass filter); *Bottom right panel:* red channel / Eu3+ luminescence (detected with APD and a 590-680 nm band-pass filter); merge of LysoView488 and Eu^{3+} emission. Scale bars correspond to 10 µm. In the green channel (Lysoview488), signal intensity was scaled so that autofluorescence is not shown.

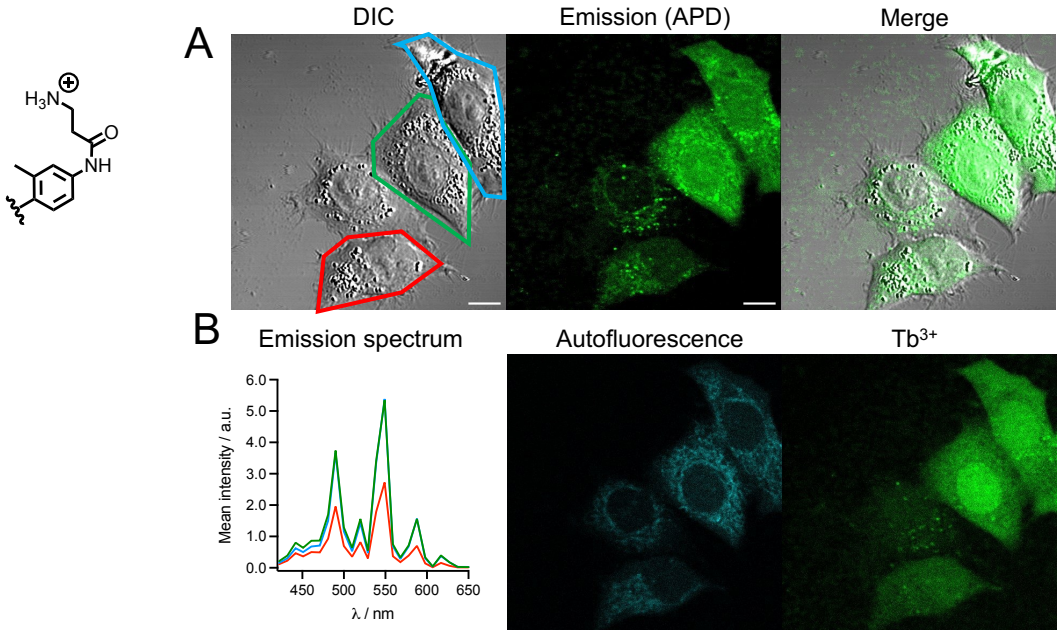

Fig. S16. 2PM imaging (λ_{ex} = 720 nm) of living HeLa cells incubated 1 h with dTAT[Tb·L-^{Me}Ar-NHβAla(+)] (10 µM) in RPMI medium. (A) *Left panel:* DIC image; *Middle panel*: luminescence (detected with APD) image; *Right panel:* merge. Scale bars correspond to 10 µm. (B) *Left panel:* 2P-excited emission spectra (detection with PMT) of cells surrounded in red, green and blue in panel A; *Middle and right panels:* autofluorescence and Tb^{3+} emission maps obtained by linear unmixing of 2P-excited spectral images recorded with the PMT.

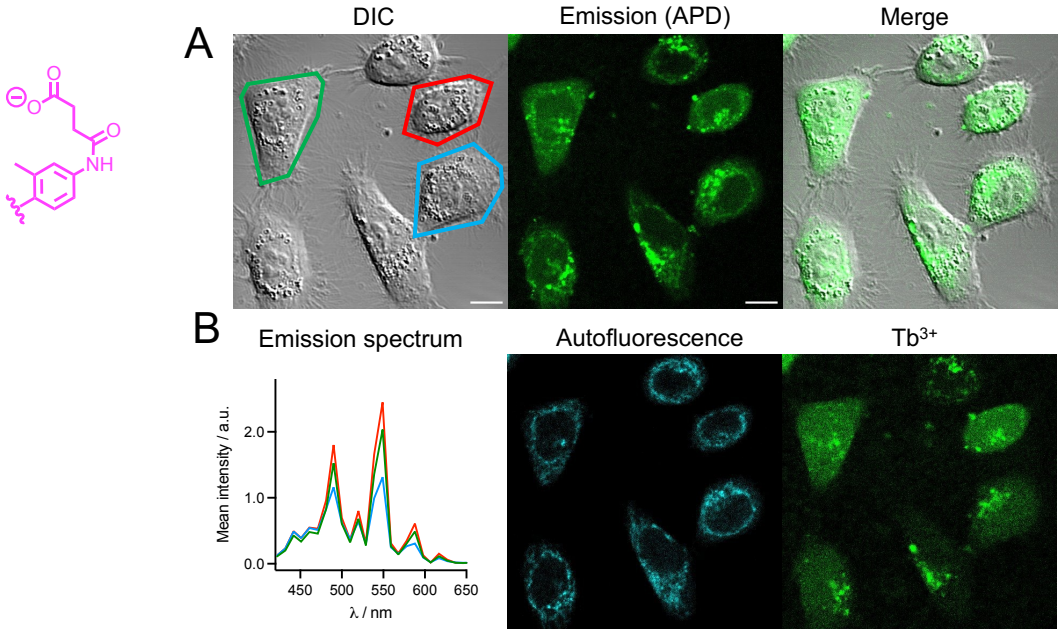

Fig. S17 2PM imaging (λ_{ex} = 720 nm) of living HeLa cells incubated 1 h with dTAT[Tb·L-^{Me}Ar-NHSuc(–)] (10 µM) in RPMI medium. (A) *Left panel:* DIC image; *Middle panel*: luminescence (detected with APD) image; *Right panel:* merge. Scale bars correspond to 10 µm. (B) *Left panel:* 2P-excited emission spectra (detection with PMT) of cells outlined in red, green and blue in panel A; *Middle and right panels:* autofluorescence and Tb^{3+} emission maps obtained by linear unmixing of 2P-excited spectral images recorded with the PMT.

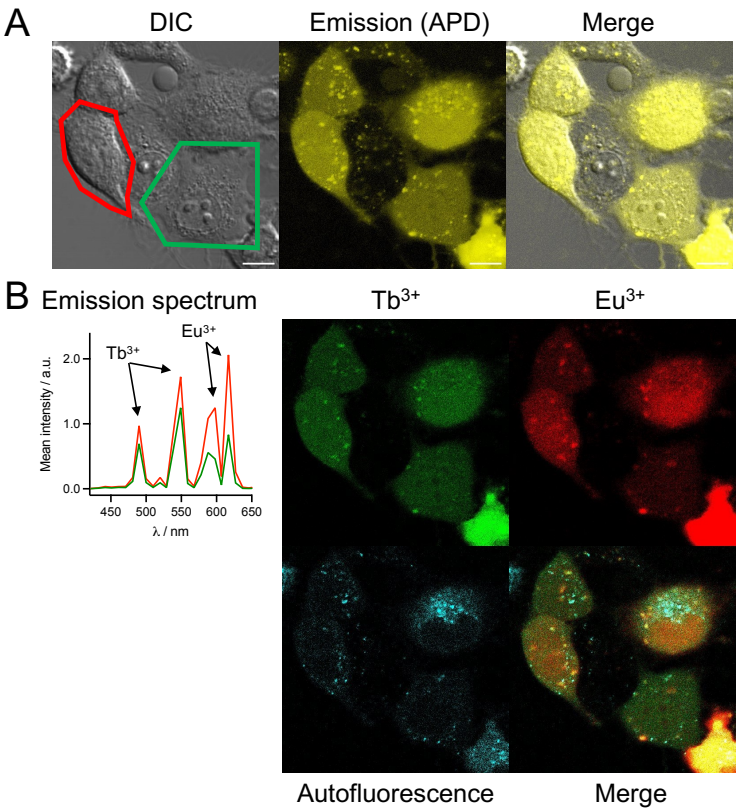

Fig. S18 2PM imaging (λ_{ex} = 720 nm) of living HeLa cells incubated 1 h with dTAT[Tb·L-^{Me}Ar-NHSuc(–)] (10 µM) and dTAT[Eu·L-Ar-NHAc] (5 µM) in PBS. (A) *Left panel:* DIC image; *Middle panel*: luminescence image recorded using APD; *Right panel:* merge. Scale bars correspond to 10 µm. (B) *Left panel:* 2P-excited emission spectra (detection with PMT) of cells outlined in red and green in panel A; *Right panel:* Tb^{3+}, Eu^{3+}, autofluorescence emission maps obtained by linear unmixing of 2P-excited spectral images recorded with the PMT and merge of the three.

Cytotoxicity

MTT proliferation assay: Inhibition of cell proliferation by dTAT[Ln·L] conjugates was measured by a MTT assay. HeLa cells were seeded into 96-well plates (3×10^3 cells per well) in 100 µL of culture medium (RPMI with 10% of fetal calf serum). After 24 h, cells were washed with PBS three times, then treated with compound dissolved at various concentrations in RPMI medium (without phenol red and without serum) during 2 h. A control with culture medium only was prepared also. Following incubation of the cells with the samples, the solution was discarded, the cells were washed twice with PBS and fresh culture medium was added to the wells. After 24 h at 37 °C, plates were centrifugated for 5 min at 400 g. The medium was then discarded and replaced with fresh culture medium containing MTT (0.5 mg/mL, Euromedex, Mundolsheim, France). After 3 h at 37 °C, 100 µL of solubilizing solution (10% Triton-X100, 0.1 M HCl, in isopropanol) were added in each well. Plates were incubated at room temperature under shaking until solubilization of water insoluble purple formazan crystals. Absorbance was then measured on an ELISA reader (Tecan, Männedorf, Switzerland) at a test wavelength of 570 nm and a reference wavelength of 650 nm. Absorbance obtained by cells in control medium was rated as 100 % cell survival. Each data point is the average of three independent experiments. Data were then fitted using GraphPad Prism to determine IC50 values.

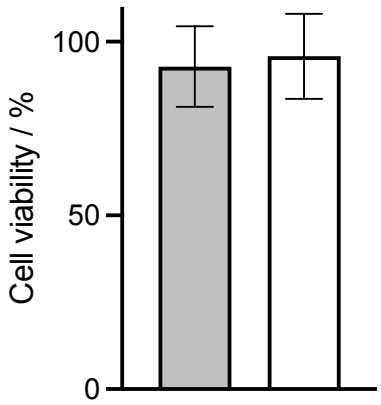

Fig. S19 Cell viability by MTT proliferation assay for co-incubations. (grey) dTAT(Tb·L-^{Me}Ar-NHβAla(+)) 10 µM + dTAT(Eu·L-Ar-NHAc) 3 µM; (white) dTAT(Tb·L-^{Me}Ar-NHSuc(–)) 10 µM + dTAT(Eu·L-Ar-NHAc) 5 µM. Error bars correspond to SD.

References

[1] B. Jagadish, T. J. Ozumerzifon, S. A. Roberts, G. B. Hall, E. A. Mash, N. Raghunand, *Synth. Commun.* **2014**, *44*, 441–449.

[2] V. Placide, A. T. Bui, A. Grichine, A. Duperray, D. Pitrat, C. Andraud, O. Maury, *Dalton Trans.* **2015**, *44*, 4918–4924.

[3] J. W. Clary, T. J. Rettenmaier, R. Snelling, W. Bryks, J. Banwell, W. T. Wipke, B. Singaram, *J. Org. Chem.* **2011**, *76*, 9602–9610.

[4] G. T. Lee, X. Jiang, K. Prasad, O. Repič, T. J. Blacklock, *Adv. Synth. Catal.* **2005**, *347*, 1921–1924.

[5] F. Mo, Y. Jiang, D. Qiu, Y. Zhang, J. Wang, *Angew. Chem., Int. Ed.* **2010**, *49*, 1846–1849.

[6] S. A. Palasek, Z. J. Cox, J. M. Collins, *J. Pept. Sci.* **2007**, *13*, 143–148.

[7] N. Thieriet, J. Alsina, E. Giralt, F. Guibe, F. Albericio, *Tetrahedron Lett.* **1997**, *38*, 7275–7278.

[8] J.-H. Choi, G. Fremy, T. Charnay, N. Fayad, J. Pécaut, S. Erbek, N. Hildebrandt, V. Martel-Frachet, A. Grichine, O. Sénèque, *Inorg. Chem.* **2022**, *61*, 20674–20689.

[9] A. Beeby, I. M. Clarkson, R. S. Dickins, S. Faulkner, D. Parker, L. Royle, A. S. de Sousa, J. A. G. Williams, M. Woods, *J. Chem. Soc., Perkin Trans. 2* **1999**, 493–504.

[10] A. M. Brouwer, *Pure Appl. Chem.* **2011**, *83*, 2213–2228.

[11] U. Resch-Genger, K. Rurack, *Pure Appl. Chem.* **2013**, *85*, 2005–2013.

[12] S. de Reguardati, J. Pahapill, A. Mikhailov, Y. Stepanenko, A. Rebane, *Opt. Express* **2016**, *24*, 9053–9066.

[13] A. Grichine, A. Haefele, S. Pascal, A. Duperray, R. Michel, C. Andraud, O. Maury, *Chem. Sci.* **2014**, *5*, 3475–3485.